The Spitzer c2d Survey of Large, Nearby, Interstellar Clouds: VII. Ophiuchus Observed with MIPS

Deborah L. Padgett[1,2], Luisa M. Rebull[1], Karl R. Stapelfeldt[3], Nicholas L. Chapman[4], Shih-Ping Lai[4,5,6], Lee G. Mundy[4], Neal J. Evans II[7], Timothy Y. Brooke[1], Lucas A. Cieza[7], William J. Spiesman[7], Alberto Noriega-Crespo[1], Caer-Eve McCabe[1,3] Lori E. Allen[8], Geoffrey A. Blake[9], Paul M. Harvey[7], Tracy L. Huard[8], Jes K. Jørgensen[8,10], David W. Koerner[11], Philip C. Myers[8], Annelia I. Sargent[12], Peter Teuben[4], Ewine F. van Dishoeck[13], Zahed Wahhaj[11,14], & Kaisa E. Young[7,15]

ABSTRACT

We present maps of 14.4 deg^2 of the Ophiuchus dark clouds observed by the *Spitzer* Space Telescope Multiband Imaging Photometer for *Spitzer* (MIPS).

[1]Spitzer Science Center, MC 220-6, California Institute of Technology, Pasadena, CA 91125 USA

[2]email: dlp@ipac.caltech.edu

[3]Jet Propulsion Laboratory, MS 183-900, 4800 Oak Grove Drive, Pasadena, CA 91109

[4]Department of Astronomy, University of Maryland, College Park, MD 20742

[5]Institute of Astronomy and Department of Physics, National Tsing Hua University, Hsinchu 30043, Taiwan

[6]Academia Sinica Institute of Astronomy and Astrophysics, P.O. Box 23-141, Taipei 106, Taiwan

[7]Department of Astronomy, University of Texas at Austin, 1 University Station C1400, Austin, TX 78712

[8]Harvard-Smithsonian Center for Astrophysics, 60 Garden Street, MS42, Cambridge, MA 02138

[9]Division of Geological and Planetary Sciences, MS 150-21, California Institute of Technology, Pasadena, CA 91125

[10]Current address: Argelander-Institut fr Astronomie Auf dem Hgel 71 D-53121 Bonn Germany.

[11]Department of Physics and Astronomy, Northern Arizona University, NAU Box 6010, Flagstaff, AZ 86011-6010

[12]Division of Physics, Mathematics, and Astronomy, MS 105-24, California Institute of Technology, Pasadena, CA 91125

[13]Leiden Observatory, PO Box 9513, NL 2300 RA Leiden, The Netherlands

[14]Current address: Institute for Astronomy, University of Hawaii, 2680 Woodlawn Drive, Honolulu HI 96822-1897

[15]Current address: Department of Physical Sciences, Nicholls State University, Thibodaux, Louisiana 70301

These high quality maps depict both numerous point sources as well as extended dust emission within the star-forming and non-star-forming portions of these clouds. Using PSF-fitting photometry, we detect 5779 sources at 24 μm and 81 sources at 70 μm at the 10σ level of significance. Three hundred twenty-three candidate young stellar objects (YSOs) were identified according to their positions on the MIPS/2MASS K versus K$-$[24] color-magnitude diagrams as compared to 24 μm detections in the SWIRE extragalactic survey. We find that more than half of the YSO candidates, and almost all the ones with protostellar Class I spectral energy distributions, are confined to the known cluster and aggregates.

Subject headings: infrared:stars - infrared:ISM - ISM:clouds - ISM: individual (L1688, L1689, L1709) - stars:formation stars: circumstellar matter - stars:pre-main sequence

1. Introduction

The Ophiuchus molecular cloud complex is one of the most well-known regions of nearby active star formation. For the Lynds 1688 cloud alone, *Simbad* lists 770 references as of summer 2006. The clouds ($\alpha = 16^h28^m06^s$, $\delta = -24°32.5'$) are considered to be at a distance of 125±25 pc (de Geus et al. 1989), although more distant estimates are seen in the literature (145 pc, de Zeeuw et al. 1999; 160 pc, Chini 1981). The stellar population of the Ophiuchus clouds has been the subject of many imaging surveys (Grasdalen, Strom, & Strom 1973; Vrba et al. 1975; Wilking & Lada 1983; Lada & Wilking 1984; Rieke et al. 1989; Strom et al. 1995; Barsony et al. 1989, 1997, 2005; Greene et al. 1992; Comeron et al. 1993; Bontemps et al. 1998; Allen et al. 2002; Duchêne et al. 2004; etc.) and spectroscopic surveys (Bouvier & Appenzeller 1992; Greene et al. 1995; Martín et al. 1998; Wilking et al. 1999; Luhman et al. 1999; Cushing et al. 2000; Wilking et al. 2005; Natta et al. 2006; etc.). Many thousands of sources have been cataloged at near-IR wavelengths; however, the majority of these sources are extincted background stars (Barsony et al. 1997).

L1688 contains the most famous star-forming cluster in this region with of order 100 stars <1 Myr old, including several extremely young Class 0 - I sources (Bontemps et al. 2001; Duchêne et al. 2004; Haisch et al. 2002; and many older studies). The vicinity of this cluster is covered in bright and dark nebulosity, and Herbig-Haro flows criss-cross the entire region (Gomez, Whitney, & Wood 1998; Phelps et al. 2006). Most of the known young stellar objects are found within an embedded cluster only a few parsecs in extent, making Ophiuchus one of the higher density environments among the nearby low mass star formation regions (Grasdalen, Strom, & Strom 1973; Wilking & Lada 1983; Wilking & Lada 1989, etc.). It is

also a region forming intermediate mass stars, bridging the gap between Taurus (a region of low-mass, isolated star formation) and Orion (a dense cluster with massive O stars). In Ophiuchus, the principal region of low mass star formation is in the vicinity of several intermediate to high mass stars of the Sco OB1 association (de Zeeuw 1999), and a number of A and B stars appear to be embedded within the cloud (Klose 1986; Devito & Haywood 1998).

The molecular material in the Lynds 1688 and 1689 clouds extends far beyond the boundaries of the extant surveys for YSOs. To the southeast of L1688 is the L1689 cloud, which extends to the east in the L1712 and L1729 streamers. Only a few isolated Young Stellar Objects (YSOs) are known in this fairly massive cloud, leading Nutter, Ward-Thompson, & André (2006) to dub it "the dog that didn't bark." Their submm continuum mapping survey indicates that most of the mass of L1689 resides in distributed cloud material rather than dense cores, unlike L1688, and suggests that the proximity of L1688 to σ Sco explains its much greater star formation efficiency. Filamentary clouds (L1709, L1740, and L1744+L1755+L1765 = "Oph North") also extend to the northeast of L1688. To date, these clouds are lacking in high resolution mid-IR surveys to identify and characterize their YSO content. Only the IRAS and 2MASS surveys exist for these regions. The ISOCAM survey of Oph covered only 0.7 square degrees (Bontemps et al. 1998). Those authors claim that most of the YSOs outside of this central region are weak-line and post T Tauri stars and, indeed, this is generally true based on only the IRAS and ROSAT studies of the region. The current study using *Spitzer* is capable of detecting low luminosity Class 0 - III infrared sources throughout a much larger surveyed area.

The Ophiuchus molecular cloud complex is one of five star-forming regions observed with the *Spitzer* Space Telescope (*Spitzer*) as a part of the "Molecular Cores to Planet- forming Disks" (c2d) Legacy project (Evans et al. 2003). The goal of this survey is to characterize the circumstellar material of young stars and substellar objects in these clouds. This paper is one in a series which present the c2d large cloud mapping results made with *Spitzer's* Infrared Camera (IRAC) and Multi-band Imaging Photometer for *Spitzer* (MIPS). Others in the series report results for Chamaeleon II (MIPS: Young et al. 2005; IRAC: Porras et al. 2007), Lupus (MIPS: Chapman et al. 2007), Perseus (MIPS: Rebull et al. 2007; IRAC: Jørgensen et al. 2006), and Serpens (IRAC: Harvey et al. 2006; MIPS: Harvey et al. 2007). These papers endeavor to present the results for each cloud and instrument in a standard format. Although the current work principally discusses the Ophiuchus MIPS maps, data from IRAC are also integrated into sections regarding source classification and individual objects. The IRAC results for Ophiuchus will be presented in Allen et al., in preparation.

The c2d MIPS survey of Ophiuchus attempts to determine the importance of a more

distributed mode of star formation in the less-studied areas outside the Oph core by covering more than 13.8 square degrees in the region where $A_V \geq 5$ at sensitivity levels considerably better than that of ISOCAM at mid-IR wavelengths and many orders of magnitude better than IRAS and ISOPHOT at far-IR wavelengths. The three MIPS filters at 24, 70, and 160 μm are ideally suited for linking the circumstellar environment of individual stars to the interstellar environment of the cloud. The MIPS 24 μm band is especially useful for identifying stars with infrared excess since stellar photospheric emission has decreased by two orders of magnitude from the blackbody peak, increasing the contrast with peak emission from cool dust. Thus, stars with warm young disks are generally extremely bright at 24 μm relative to stars without disk emission. MIPS 70 μm emission is also seen in the brighter envelopes and disks and in interstellar regions where dust is heated by young stars. MIPS 160 μm traces cool dust in both circumstellar and interstellar regions, similar to the IRAS 100 μm band. The combination of MIPS data with surveys at other wavelengths enables detailed studies of YSO spectral energy distributions (SEDs) and the cloud environment. The most recent millimeter continuum maps of this region have been presented by Young et al. (2006), who used CSO/Bolocam to map the region observed by *Spitzer*. High quality millimeter molecular line maps of Ophiuchus also covering the *Spitzer* survey are available from the COMPLETE team (Ridge et al. 2006).

In this paper, we first present the *Spitzer* MIPS observations of Ophiuchus (§2). Following the observations section, we discuss results, including multi-wavelength images (§3.1), MIPS source counts (§3.2), bandmerging with IRAC and 2MASS (§3.3), and a variety of color-color and color-magnitude diagrams (§3.4). Then we investigate recovery of IRAS objects (§3.5) and variability at 24 μm on timescales of 3-8 hours in Section 3.6. We have highlighted the spectral energy distributions (SEDs) and imaging of several individual objects in Section 4.1. We then discuss the distribution of infrared excess sources in Ophiuchus and comment on the degree of clustering found throughout the region (§4.2). Finally, we summarize our main points in §5.

2. Observations and Data Reduction

2.1. MIPS

The MIPS observations of Ophiuchus were conducted on 2004 March 18-19 and covered 13.8 square degrees. Two off-cloud fields totalling 0.6 square degrees were observed with the intention of characterizing the background starcounts. The center of this large map is roughly at α, δ (J2000) = $16^h33^m18.0^s$ $-24°15'$, or l, b=354°, +16.0°, or ecliptic coordinates (J2000) 251°, $-2.5°$. The area mapped with MIPS completely covers the c2d IRAC map

regions in Ophiuchus, which included all the cloud area above the A_V=5 contour. The combination of the cloud being extended perpendicular to the MIPS scan direction, and the fixed scan length options available for use with MIPS, dictated that the area covered by the Ophiuchus MIPS maps is more than twice the area mapped with IRAC.

These observations were part of Spitzer program id 177; the AORKEYs appear in Table 1. Fast scan maps were obtained at two separate epochs separated by a few hours. At each epoch, the spacing between adjacent scan legs was 240″. The second epoch observation was offset 125″ in the cross-scan direction from the first, to fill in the 70 μm sky coverage which was incomplete at each individual epoch. Furthermore, the second epoch scan was also offset 80″ from the first in the scan direction, to maximize 160 μm map coverage. These mapping parameters resulted in every part of the map being imaged at two epochs at 24 μm and only one epoch at 70 and 160 μm, with total integration times of 30 sec, 15 sec, and 3 sec at each point in the map (respectively). Even with this strategy, the 160 μm maps have some gaps, which makes point source photometry especially uncertain at this wavelength. In addition, the 160 μm array saturated in the region at the center of the L1688 cloud.

Figure 1 shows the region of 3-band coverage with MIPS, and the 4-band coverage with IRAC. In addition to the c2d data, smaller MIPS maps of Ophiuchus were obtained by the *Spitzer* Guaranteed Time Observers. To maintain uniform sensitivity in our maps, these data were not incorporated into the current study.

The observations were conducted at two separate epochs separated by about 3 to 8 hrs to permit asteroid removal in this low ecliptic latitude ($\sim 0°$) field. Study of the asteroid population in Taurus at a similar ecliptic latitude (0 - 7 deg) indicates there are roughly 250 asteroids per square degree with 24 μm flux densities ≥ 1.6 mJy (Stapelfeldt et al. 2006). By extracting sources separately from the two epochs and comparing the source lists, transient sources were eliminated from our MIPS catalog. This observation technique also enables a study of 24 μm source variability on a timescale of several hours; see Section 3.6.

The MIPS observations of Ophiuchus included two small off-cloud regions with total area of 0.66 square degrees, in addition to the 13.8 square degrees of the main map. These were intended to provide statistics on the stellar and extragalactic background. However, these regions were found to be too small and sparse to yield reliable statistics. In addition, one of the fields inadvertantly included the large globular cluster M4, which severly biases its source counts. Thus, we do not utilize these offcloud regions; instead, we compare our statistics to the 6.15 sq. deg. the ELAIS N1 field mapped by the Spitzer Wide-area InfraRed Extragalactic ("SWIRE") survey (Shupe et al. 2006), which was re-reduced and analyzed using the c2d pipeline. In the low ecliptic latitude Ophiuchus region, MIPS source counts are dominated by asteroids and the extragalactic background rather than stellar photospheres,

and thus a comparison to the SWIRE field is invaluable despite its considerably different Galactic latitude. However, we do include the off-cloud fields (OC1,2) in the table of statistics (see Section 3.2).

We started with the SSC-pipeline produced basic calibrated data (BCDs), version S11.4. Each MIPS channel was then processed differently and therefore is discussed separately below. Additional detail on the data reduction process can be found in Young et al. (2005), Chapman et al. (2007), and Rebull et al. (2007).

Standard c2d pipeline processing was used for MIPS-24 (Young et al. 2005, Evans 2005). After some corrections for non-uniform readout variations (jailbars) were applied to individual frames ("basic calibrated data" or BCDs), these data were transformed into single epoch mosaics using the SSC MOPEX software (following Chapman et al. 2007). Source lists were extracted using "c2dphot" (Harvey et al. 2006) to measure flux densities using point spread function (PSF) fitting. The final working 2005 catalog as assembled consists of all detections at MIPS-24 with high quality c2d catalog detection flags (Evans et al. 2005) and detections at both epochs. While resulting in a shallower survey than would be possible using other combinations of flags, this ensures that no asteroids are included in the final catalog. The zero point used to convert these flux densities to magnitudes was 7.14 Jy, based on the extrapolation from the Vega spectrum as published in the MIPS Data Handbook. There were 5779 total point sources detected at 24 μm meeting our criteria, ranging from 0.672 to 3910 mJy. Note that the spatial resolution of MIPS-24 is $\sim 6''$, with a 2.55$''$ pixel size.

For the MIPS-70 data, we started with the automated pipeline-produced BCDs, both the filtered and unfiltered products. Then individual BCDs were mosaicked into one filtered and one unfiltered mosaic using the SSC software MOPEX (Makovoz et al. 2006). We performed source detection and extraction using MOPEX/APEX on the entire mosaic. The source list was cleaned for instrumental artifacts via manual inspection of the 70 μm image and comparison to the 24 μm image; e.g., if there was some question as to whether a faint object seen at 70 μm was real or an instrumental artifact, and comparison to the 24 μm image revealed a 24 μm source, then the 70 μm object was judged to be a real source. About 80% of the 70 μm objects had identifiable counterparts at 24 μm. The zero point used to convert the flux densities to magnitudes was 0.775 Jy, based on the extrapolation from the Vega spectrum as published in the MIPS Data Handbook. There were 81 total point sources detected at 70 μm. There were 19 objects brighter than 4 Jy, for which we employed aperture photometry with a 32$''$ aperture and a 17% aperture correction. Note that the spatial resolution of MIPS-70 is $\sim 18''$.

The 160 μm MIPS band presented challenges for point source extraction due to scattered gaps in the map coverage. A small amount of smoothing was applied to the data in order to

fill gaps. Then APEX was used to find sources thoughout the image. Because of the large saturated region in L1688 and the highly structured nature of the bright diffuse emission, few isolated point sources were identified in our study. The zero point used to convert the flux densities to magnitudes was 0.159 Jy, based on the extrapolation from the Vega spectrum as published in the MIPS Data Handbook. There were 8 total point sources detected at 160 μm, ranging from 876 mJy to 19 Jy. About 60% of the 160 μm objects had identifiable counterparts at 24 and 70 μm. The extreme brightness and saturation of the 160 μm diffuse emission made detection of 160 μm sources impossible in the most densely populated regions of the cluster. Finally, note that the spatial resolution of MIPS-160 is $\sim 36''$.

Although this paper is primarily about point sources, there is extensive extended emission in all three MIPS channels throughout the MIPS maps. The diffuse emission ranges in brightness from $50 - 570$ MJy/sr at 24 μm where the low value is set by the overall zodiacal emission in this low ecliptic latitude region. The 70 μm extended emission ranges in surface brightness from $\sim$30 $-$ 5000 MJy/sr, while the 160 μm extended emission varies from 45 $-$ 400 MJy/sr (with the central region of L1688 being saturated). This extreme background variation unfortunately results in highly non-uniform point source detection sensitivity in our survey. Our region of worst sensitivity coincides with the central core of L1688 where the most intense past studies have been performed. Thus, our *Spitzer* c2d survey should be considered complementary to past ISO and ground based IR studies in Oph.

Because a large cloud complex is encompassed by our maps and the population of the individual clouds are known to have substantially different characteristics, we have chosen to separate out the properties of stars in L1688, L1689, L1709, and the L1712+L1729 filaments; see Figure 1. In addition, we have separated out the properties of the disconnected northern filaments (L1744+L1755+L1765), which we identify as Oph North. The above regions were defined as rectangles shown in Figure 1 with corners given in Table 2.

2.2. CSO Sharc II

Several L1709 sources were observed at 350 μm, using Sharc II at the Caltech Submillimeter Observatory (CSO) on 2007 April 23, 25 and 26th. Sharc II is a 12×32 bolometer array, with a pixel size of $4.85''$ and a field of view of $2.6'$ by $0.97'$. The Dish Surface Optimization System (DSOS) was used throughout the run, providing a stable beam, with a FWHM of $\sim 8''$ at 350 μm. Sub-mm conditions were excellent throughout the run, with τ_{225} ranging from 0.03 to 0.045. Target observations were interspersed with observations of IRAS 16293-2422 and Callisto, which were used for both pointing and flux correction. The data were reduced using the CSO data pipeline CRUSH, and relative aperture photometry on the

sources obtained. The measurement uncertainties include the flux calibration uncertainty, which is typically on the order of 20%.

3. Results

3.1. Multi-wavelength images

The MIPS 24 μm mosaic (Figure 2) shows a great deal of diffuse nebulosity and many bright point sources. The central region of L1688 (Figure 3) is dominated by nebulosity near the early type stars (S1, SR3) embedded in the cloud. The S1 source is saturated in the MIPS 24 μm image, but the peak appears extended, and it is surrounded by a complex cometary nebula opening toward the northeast. The B star SR 3 also appears as a resolved nebulosity at 24 μm as do the more embedded early-type objects WL 16 and WL 22. The WL 22 nebula has a central core with FWHM of 18″ and an outer cometary morphology extending to radii of 30″ . The WL 16 nebula is more elongated, 2′ by 35″ along PA 10° - 50° from the major axis of the PAH disk reported by Ressler and Barsony (2003). An elliptical ring of emission about 1′ across is centered on a point source near the position of ISO-Oph 125 and ISO-Oph 124 (YLW 12B and 12A; spectral types F7 and M4 Greene & Meyer 1995; Luhman & Rieke 1999). Two other point sources within this ring are also detected at the positions of ISO-Oph 128 and ISO-Oph 129. South of these sources, the HD 147889 star appears only as a faint point source against some of the brightest part of the central Oph nebulosity and shows a purely photospheric SED. This confirms that the large FIR excesses assigned to this source by the IRAS PSC are most likely due to interstellar emission, rather than circumstellar material. Ground based photometry of this source (Lada, Wilking, & Young 1989) also has suggested a lack of circumstellar material in this system. However, HD 148579 (B9V) south of L1689 has a resolved 24 μm nebula, as does nearby HD 148605 (B3V). Interestingly, these stars, which are apparently adjacent to or embedded in cloud material, have not excited the interstellar nebulosity to the same degree associated with the early type stars in the central cluster. The 24 μm mosaic also shows a surprising amount of "dark" nebulosity (i.e., absorbing perhaps 80% of the background illumination, in the vicinity of the L1688 cluster and extending towards L1689. One of the 24 μm dark cloudlets is shown in Figure 4.

The longer wavelength MIPS mosaics are shown in Figures 5 and 6. The 70 μm mosaic still shows striations from the detector history effects which are not entirely removed in the pipeline processing for each scan leg. Contributing to this appearance is the fact that the map was filled by interleaving observations at two different epochs. Despite the cosmetic inperfections, the MIPS 70 μm map clearly shows that the diffuse emission at this wavelength

is brightest in the L1688 region and in the area extending from northwest to southwest of the central cluster. The COMPLETE CO maps of the Oph clouds (Ridge et al. 2006) show that this region of Oph West consists of generally tenuous cloud material with a few interspersed clumps. It is possible that these regions are bright in the long-wavelength MIPS bands because they on a direct line of sight to the young B stars in the central cluster and are heated by them. S1, WL 16, WL 22, and YLW 12B continue to be nebulous at 70 μm as they were at 24 μm. There is also a small area of diffuse nebulosity adjacent to HD 148605. The sources IRAS 16293-2422 and IRAS 16288-2450 are also prominent at this wavelength. The 160 μm mosaic (Figure 6) shows the same L1688 west dust emission features as the 70 μm image. However, the cold dust in L1689 and the L1712+1729 filaments becomes prominent at this wavelength. Young et al. (2006) showed that there are some weak millimeter sources in these filaments. The central region of L1688 is saturated in the MIPS 160 μm image. Figure 7 shows a 3-color image with all three channels of MIPS included.

3.2. Source Counts

MIPS source counts in Ophiuchus are a combination of cloud members, foreground/background stars in the galaxy, and the extragalactic background. An excess of sources above comparison regions outside the clouds implies the presence of young stars with disks. Figure 8 shows the observed Ophiuchus 24 μm differential source counts in comparison to observed source counts from the SWIRE ELAIS N1 extragalactic field (solid lines), and to the prediction for Galactic star counts in the IRAS 25 μm band from the Wainscoat et al. (1992) model provided by J. Carpenter (2001, private communication; dashed lines). Aside from L1688, all of the other regions have negligible levels of excess 24 μm source counts, indicating only small numbers of young stars are present in these fields. L1709 has a modest excess above 10 mJy. These plots indicate that only L1688 has a substantial young population relative to the various foreground/background sources expected in the field.

Figure 9 shows 70 μm source counts in Ophiuchus, along with extragalactic background counts from the SWIRE ELAIS N1 field. At the low sensitivity of our 70 μm measurements, detection of normal stellar photospheres will be negligibly rare; thus, comparions with Galactic star counts are not needed. Clearly, given the high backgrounds and small number of cataloged 70 μm sources, we are dealing with small number statistics. However, the plots do show significantly more sources at bright flux density levels for the regions L1688, L1689, and possibly L1709 than would be found from the extragalactic background. For L1688, the excess sources extend down to 200 mJy, while for the other two regions, the excess above background starts at about 300 mJy. In the extended cloud outside the clusters, a slight

excess in source counts might be present above a flux density of 400 mJy. Note that the depth of 70 μm extractions is greatest in the Oph North field where the diffuse background is lowest. In this field, the 70 μm source counts follow the SWIRE survey curve to the point where the greater SWIRE sensitivity diverges from the c2d sensitivity.

3.3. Bandmerging with IRAC and 2MASS

The IRAC data for the c2d Ophiuchus field (covering $\sim$6.8 square degrees) will be described in Allen et al. (2008), and these data (as bandmerged with the MIPS sources) were included in our final catalog. Our MIPS map covers more than twice the area of the IRAC map. In the $A_V > 5$ region with full MIPS and IRAC coverage, there are 2608 MIPS-24 point sources, 88% of which have an counterpart in at least one IRAC band; 31 70 μm point sources, all but one of which have an IRAC counterpart; and six 160 μm point sources, all with IRAC counterparts. The wide variation in resolution between IRAC ($\sim$2″ at 3.6 μm) and MIPS (6″ at 24 μm, 18″ at 70μm, 36″ at 160 μm) leads to potential confusion of several IRAC objects within a single MIPS beam. Details of the bandmerger are given in Evans et al. (2007) (c2d Delivery Document). For the total MIPS map region, the above source counts approximately double; see Table 3. The c2d source catalog containing all Oph *Spitzer* sources can be found at: http://data.spitzer.caltech.edu/popular/c2d/20051220_enhanced_v1/Oph/

Near-IR JHK_s data from 2MASS (Cutri et al. 2003) were also used in constructing our catalog. The 2MASS data obviously covered the entire region of the MIPS map, but to a shallower depth than the IRAC observations, so only 45% of the MIPS-24 sources have 2MASS K counterparts, similar to the fraction seen in the Cham II catalog (Young et al. 2005).

3.4. Color-Magnitude and Color-Color Plots

For relatively bright sources, K_s versus $K_s-[24]$ can be used to separate potential YSOs from stars and most extragalactic sources. This metric has been used in a variety of *Spitzer* papers to identify stars with infrared excess (Gorlova et al. 2004, Padgett et al. 2004, Padgett et al. 2006, Rebull et al. 2007, etc.). Stellar photospheres without excess are clustered around $K_s-[24] = 0$. If $K_s-[24] > 2$, then a strong excess is present at 24 μm. Most extragalactic sources are fainter than $K_s = 14$.

Figure 10 presents K_s versus $K_s-[24]$ color-magnitude diagrams for L1688, L1689, L1709, the L1712+L1729 filament, Oph North, the rest of the cloud, and the extragalactic

SWIRE ELAIS N1 field. Note that sources that appear to be pure photospheres appear in gray. SWIRE 24 μm sources tend to congregate in two groups: namely, main sequence photospheres at color of zero and galaxies at faint K magnitudes and colors of 6 – 8. Thus, $K_s-[24]$ plots help to define regions of color-magnitude space which are likely to be affected by extragalactic sources seen through the cloud. In Figure 10 dashed lines (from right to left) denote the divisions between Class I, flat, Class II, and Class III objects following Rebull et al. (2007); in brief, we can use the observed $K_s-[24]$ colors and assign an α index following Greene et al. (1994). Note that the formal Greene et al. classification puts no lower limit on the colors of Class III objects (thereby including those with SEDs resembling bare stellar photospheres, and allowing for other criteria to define youth). In our case, since we know little about many of these objects, in an attempt to limit contamination from foreground/background stars (and background galaxies), we have imposed the additional constraint that $K_s-[24]>2$, and $K_s<14$. Note that there are certainly true young cluster members that do not meet these (conservative) criteria, but identifying them (and separating them from the galaxies) is beyond the scope of this paper. Allen et al. (in preparation) will discuss the combined IRAC and MIPS SEDs and present a list of cloud members.

Interstellar and circumstellar reddening could plausibly affect the location of sources on the K_s versus $K_s-[24]$ diagram. To test this possibility, we used the extinction law derived from *Spitzer* lines of sight through Ophiuchus (Flaherty et al. 2007) to produce a reddening vector in Figure 10. The vector depicts the effects of five magnitudes of K band extinction, which moves a star toward the lower right. Note that unlike the SWIRE sources, which show a well-defined main sequence at $K_s-[24] = 0$, almost all of the Ophiuchus sources show a displacement toward redder colors. Given the high extinctions throughout this region, many of the apparently small excess sources in L1712+L1729 and "rest of cloud" areas may simply be reddened photospheres. In addition, Class II sources could plausibly be reddened into the Class I zone. Thus, in regions of very high extinction, classification of YSOs based on even long wavelength MIPS data is complicated by reddening effects.

Table 4 provides statistics on the number of sources classified by $K_s-[24]$ as YSOs in the various subregions of the Ophiuchus map. The Oph North and off-cloud fields resemble the SWIRE regions, with most sources clumped in the photospheric and faint galaxy region of the diagram. The L1712+1729 filament shows a few more bright photospheres with small excesses than Oph North plus three potential Class II sourcs. L1709 and L1689 have a higher frequency of Class IIs than the filament, as well as a few flat and Class I SEDs. Although the number of sources in L1709 is small, this region actually has the highest fraction of Class I + flat spectrum sources in the region. These dense clouds also show fewer sources in the extragalactic clump at faint K_s and large $K_s-[24]$ due to their small area and bright 24 μm diffuse emission. Finally, the L1688 region has a high fraction of flat and Class I SED sources

(27%), and it dominates the region for sheer number of Class II sources (100).

Figure 11 shows the K_s versus $K_s-[70]$ plots for Ophiuchus. K_s-[70] = 0 would indicate a bare stellar photosphere in this plot. However, few if any bare stellar photospheres in this field are bright enough for detection in our very shallow MIPS 70 μm survey. Extragalactic SWIRE sources from the ELAIS N1 field are shown for comparison (grey dots). This plot is most useful for extremely bright YSOs which are saturated at 24 μm but not 70 μm. Again, L1688 dominates the number of potential YSOs and has the most objects with large excesses. These are likely to be the youngest in the sample. Other regions have only a handful of 70 μm YSOs, and the bulk are in the Class II regime with the exception of a few sources in L1709 and L1689. There is one object in L1689 with stellar or near-stellar colors out to 70 μm; it is SSTc2d 163528.6-245648, which we tentatively associate with Elias 2-83. This source plausibly may be a reddened star given the dark cloud visible in this area in the MIPS 24 μm image. All the 70 μm sources in Oph North are consistent with extragalactic background sources, except for SSTc2d 164417.8-220648, which can be identified with IRAS 16413-2201, a known carbon star NC 80 (Guglielmo et al. 1993).

Figure 12 presents a plot of [24] versus $[24] - [70]$ for the Ophiuchus clouds. In the unlikely case of a bare stellar photosphere, $[24] - [70] = 0$. Again, SWIRE sources are depicted as grey dots. Sources with large infrared excesses will have large [24]-[70] colors. This color-magnitude diagram shows the separation of YSOs from extragalactic sources and emphasizes that extragalactic 70 μm sources are only seen in the lower background regions. Although the number of sources seen in these plots is considerably smaller than in the 24 μm only plots (due to the lower sensitivity of the MIPS 70 μm channel), this color-magnitude diagram suggests confirmation of the picture of the L1688 cluster having a lower fraction of very young sources than L1709. However, it is true that a fair number of the most luminous MIPS sources in L1688 are saturated at 24 microns ($\geq$ 4 Jy), thus eliminating them from these plots. In addition, the small number of sources in L1709 makes the comparison of questionable significance. Interestingly, some low luminosity sources with large fractional excesses appear to be found outside of the described subclusters (in the "Rest of the cloud" areas). Note that the brightest objects in these plots (those with [24]$\leq$5 and [24]$-$[70]$\leq$6) appear for reference in Table 7 below.

Unfortunately, due to very high backgrounds and saturation issues, as well as the difference in sensitivity between the various MIPS arrays, very few point sources (5) have measurable detections at all three MIPS bands. Figure 13 presents a plot of [70]$-$[160] versus [24]$-$[70]. Included for comparison on this plot are colors calculated for MIPS bands from ISO SWS data for a variety of very famous well-studied embedded objects from A. Noriega-Crespo (private communication); to facilitate comparison, these are the same ob-

jects used in a similar plot in Rebull et al. (2007). The four Ophiuchus sources all lie between [70]−[160] of 2.5 to 3.5 while spanning a range of 4 magnitudes in [24]−[70]. This may be an extinction effect, since three of the five objects are located in regions of Oph with apparently high extinction even at 24 μm.

3.5. Comparison to IRAS

As in Rebull et al. (2007) for Perseus, the MIPS data for Oph offer an opportunity to assess how successful the IRAS survey was in identifying point sources in a complex region. We now explicitly compare the IRAS Point Source Catalog (PSC; Beichman et al. 1988) and IRAS Faint Source Catalog (FSC; Moshir et al. 1992) results in this region to the Spitzer c2d images and catalogs described in this paper. As for Perseus, extended emission is present in all three MIPS bands, posing a significant source of confusion to the large aperture IRAS measurements. Many of the IRAS PSC objects were detected at 60 or 100 μm only, with only upper limits at 12 and 25 μm; so even without Spitzer data, one might suspect that such sources might correspond to texture in the extended emission. As for Perseus (Rebull et al. 2007), the Spitzer data comparison clearly shows that significantly fewer spurious sources appear in the FSC than in the PSC.

A summary of the comparison of MIPS sources to IRAS sources are found in Table 5. For each IRAS PSC and FSC band, the number of IRAS detections are listed, followed by the number of these IRAS detections recovered by the MIPS 24 and 70 μm arrays, IRAS detections not found by MIPS, IRAS detections determined to be nebulosity by MIPS, and IRAS detections resolved as multiple by MIPS. It is not surprising that few of the long wavelength IRAS sources are recovered by MIPS 24 μm. About 65% of the 25 μm PSC sources are recovered as point sources in MIPS-24; only 23% of the 60 μm PSC sources are recovered at MIPS-70. The most frequent reason for sources not being retrieved is confusion by nebulosity; 23% of the 25 μm PSC sources and 57% of the 60 μm PSC sources are so affected. Surprisingly few objects are resolved into multiple sources by Spitzer. Only one 25 μm PSC detection is completely missing from MIPS-24; 16 of the 60 μm PSC detections are completely missing from MIPS-70. A list of IRAS PSC sources not cleanly recovered appears in Table 6.

The FSC does a much better job of finding short-wavelength point sources, and is *much* less confused by the nebulosity. However, the FSC does not contain any sources on the West side of the cloud due to high surface brightness in the IRAS images. All but one of the 25 μm FSC sources are recovered by Spitzer at 24 μm; the remaining source is resolved as multiple sources when viewed by MIPS. There are no 60 μm FSC high quality point sources

in this region.

While it would be interesting to study long-term far-infrared source variability in Oph, this is very difficult in practice. The vastly larger IRAS beam means that point source flux densities can include large contributions from bright background nebulosity. The different calibration approaches of the two instruments requires that any flux density comparison be made only after large color corrections are applied - corrections that can only be made accurately if the spectral slope is known across the photometric bandpasses. In addition, many sources detected by IRAS at 25 μm are near the upper end of the MIPS 24 μm dynamic range, where instrument calibration is less secure. For these reasons, we make no attempt to compare the MIPS and IRAS photometry for the sources detected in both surveys.

3.6. Time variability

Because we have two epochs of observation at 24 μm, we can look for time variability on timescales of a few hours. Figure 14 shows the ratio of flux densities determined in the two epochs as a function of mean 24 μm flux densities. It can be seen that typical variability is ∼10%, consistent with our reported measurement uncertainty. There are four points whose flux ratio (in the log) is greater than 0.45, and two whose flux ratio is less than -0.5. Out of these six sources, three fall on the edge of the map, and the apparent variability is clearly due entirely to the low redundancy and S/N at the ends of scan legs. Three additional objects fall in the L1688 region, where bright sources cause the readout dependent gain variation known as "jailbars." Two of the L1688 objects are faint and located right on top of some strong jailbars, and one is deep within the bright, extended emission. Therefore, apparent variability in all cases is entirely due to instrumental effects.

4. Discussion

4.1. Individual Objects

4.1.1. Young Stellar Objects with Extreme K_s-[24] Colors

YSO modelling indicates that some of the earliest evolutionary states of star/disk systems will be detected by *Spitzer* as point sources with extremely red colors (Robitaille et al. 2006). A search through our catalog for sources with $K_s < 12$ and K_s-[24] > 8 yielded eight sources Their SEDs are presented in Figure 15. One of these objects (SSTc2d 162623.5-242439) had been previously identified as CRBR 2322.1-1754 (Comeron et al. 1993). In that

paper, the source was detected out to Q band, but was not characterized further. In our data, this source is probably confused at 24 μm with GY21, a flat spectrum YSO a few arcsec away (Greene et al. 1994). Its SED is characteristic of an extincted stellar photosphere with an excess which appears to be present in the IRAC bands and extends to 24 μm. No 70 μm source is detected. It lies close to another YSO (Oph S2) (best seen in our 24 μm image), and thus there is potential SED confusion at longer wavelengths. Source SSTc2d 162648.4-242838 is similar, although fainter. It also appears as a binary source in the IRAC 3.6 μm band and can tentatively be identified with WL 2 (Wilking et al. 1989). Finally, SSTc2d 162737.2-244238 (GY 301) is a faint stellar source with an almost flat spectrum out to 70 μm. All of these sources appear in high extinction regions, and it appears likely that their extraordinary $K_s-[24]$ color is primarily due to extinction at the K_s band. Thus, these are likely normal flat spectrum YSOs with disks seen at very high extinctions due to location within the cloud or envelope.

4.1.2. The L1709 Aggregate and a Possible Edge-on Disk

In L1709, there is a grouping of six bright 24 μm point sources within $4.2' \times 3.3'$ (see Figure 16). SEDs for all six of these objects appear in Figure 17 and MIPS fluxes for these objects appear in Table 7. As a shorthand, numbers between 1 and 6 appear in Figure 17; the corresponding formal c2d names appear in Table 8. IRAS 16285-2358 can be identified with source 2 in Figure 17. This object was selected as a candidate YSO by Beichman et al. (1986). IRAS 16285-2355, source 4 in Figure 17, is also selected as one of the most extreme $K_s-[24]$ colors in the cloud. This well-known source (e.g., Visser et al. 2002 and references therein) shows a typical Class I or flat spectrum SED rising through the mid-IR and flattening across the three MIPS bands. It appears to be a higher luminosity version or more pole-on disk geometry of the same type of sources with extreme $K_s-[24]$ colors discussed in the previous section. Objects 1, 3, 5, and 6 in Figure 17 do not have any known counterparts in the literature. Source SSTc2d 163136.7-240420, source 5 in Figure 17, stands out for its similarity to model edge-on disks similar to such objects as HH 30 (Burrows et al. 1996). The 2MASS+IRAC part of the SED resembles a normal stellar photosphere which peaks at K, albeit a very faint one. However, its 24 μm and 70 μm fluxes are almost two orders of magnitude higher than the 8.0 μm value. Edge-on disks such as HH 30 and HK Tau/c (Wood et al. 2002) can appear in scattered light until 10 – 20 microns, suppressing both their short and long wavelength flux densities. A 3.6 μm image is presented in Figure 18.

Five of the six sources in L1709 were observed in the 350 μm continuum at the CSO. Two (L1709-3 and 4) were clearly detected and showed extended structure. For these sources, an

elliptical aperture with radius of 1′ used to calculate the flux density, excluding some of the low level extended structure in the images. The L1709-5 (SSTc2d163136.7) source is in a region of considerable structure - it appears to be sitting on a ridge of emission and shows a cometary structure extending toward the south-south-east. To the north-west (α=16 31 35.33, δ=-24 03 46.8) is another bowed extended ridge of emission, with a flux of $\sim$200 mJy. The CSO flux densities and upper limits are incorporated in the SEDs presented in Figure 17. We use the equations of Beckwith et al. (1990) to estimate lower limits on the circumstellar mass from these measurements. Presuming that the 350 micron emission is optically thin and $T_d = 100$ K, $\kappa_\nu = 0.071$, leading to lower limits on the circumstellar masses of 1.6×10^{-2} $M_\odot$ for SSTc2d163135.6-240129 (L1709-4) and 6.4×10^{-4} $M_\odot$ for SSTc2d163136.7-240420 (L1709-5).

4.1.3. L1689

The famous Class 0 source IRAS 16293-2422 appears in the L1689 part of our MIPS maps. Interestingly, the source is entirely invisible in the IRAC 8 μm image, although some of the jet and bowshock emission from the outflow is plainly visible. The source itself begins to be seen at faint levels at 24 μm, is very bright at 70 μm, and is saturated at 160 μm. A color image is shown in Figure 19. The 8 μm visibility of shocked gas very close to the invisible central source implies that the high extinction region is very confined in areal coverage, suggesting an edge-on orientation to the disk/envelope system. This source has also been observed by the *Spitzer* Infrared Spectrograph (IRS) (Jørgensen et al. 2005). In this work, the authors interpret the rapid rise in the SED as a large inner hole in an extended envelope around a protobinary. We prefer to interpret the very large slope in the SED as an extinction effect from a highly inclined disk/envelope system.

There is an aggregate of nine stars bright at 24 μm found clustered within a 5′ region within L1689. The MIPS-24 image of the aggregate is presented in Figure 20, and the *Spitzer*+2MASS SEDs for these stars appear in Figure 21. Several of these objects were also seen by ISO and discussed as part of Bontemps et al. (2001).

Padgett et al. (2004) and Rebull et al. (2007) commented upon small clusterings of sources bright at 24 found in L1228 and Perseus, respectively. While Oph does not have such aggregates in as high abundance as in Perseus, this grouping in L1689 is clearly a similar phenomenon in that there are several sources within $\sim$0.15 pc, all bright at 24 μm and with a diversity of SEDs. As can be seen in Figure 21, some sources resemble reddened photospheres with just a hint of excess at 24 μm (e.g., #1), some appear to have Class II SEDs (e.g., #8), and some have substantial excesses like Class I or flat spectrum SEDs

(e.g., #6). Source #5 has a strangely shaped SED because it is an unresolved binary at 24 μm. Source #9 is so bright at 24 μm as to leave several latents on the array (e.g., it is near saturation), so the unusual shape of the IRAC portion of the SED is likely to be a result of saturation in those bands. Object #4 is saturated at all Spitzer bands except for 70 microns. The proximity of these sources suggest that they are physically associated, despite their disparate SEDs. As in L1228 (Padgett et al. 2004), this aggregate seems to have sources at a variety of stages in their circumstellar evolution although the sources must be nearly coeval.

4.2. Clustering of YSOs in Ophiuchus

Figure 1 shows the distribution of MIPS 24 μm sources in the c2d maps. The sources appear to be randomly distributed in most of the map. However, as expected, there is a large overdensity of sources in the region around the Oph A core. Figure 22 accentuates this result, showing that relatively bright sources with 24 μm excess are strongly concentrated in the core, as well as a scattering of small groups in L1689 and northern L1688 and southern L1709. A modest number of excess sources are more widely distributed over the entirety of the L1719+1729 eastern filament, while Oph North has few bright 24 μm excess sources. The "rest of the cloud," largely concentrated to the northeast of L1688, shows some intriguing small individual sources, but no YSO aggregates.

Table 4 quantifies the degree of clustering seen by categorizing the objects with 24 μm excess. Consideration of all 24 μm sources with 2MASS associations shows that only 297 out of a total of 2590 sources are confined to the L1688 subregion. This would imply a large distributed population of potentially young sources in the cloud. However, when the selection criteria $K_s - [24] > 2, K_s < 14$ are applied, we see that more than half of the YSO candidates are confined to L1688. About 60% of the YSO candidates fall into the L1688, L1689, and L1709 regions. The clustering of sources with Class I and flat SEDs is more pronounced. A full 95% of these sources are confined to the central cluster and the L1709 and L1689 aggregates. In comparison, only 61% of the Class II candidates are located in these subregions. It is worth noting that the nature of Class I and II candidates remain unconfirmed by further study outside of the well-studied cluster and aggregates. Some percentage of these sources may well be extragalactic interlopers. Thus, star formation in the Ophiuchus clouds appears to be largely confined to the cluster and aggregates. Small aggregates of the type seen in Taurus, Lupus, and Perseus are found in the L1709 and L1689 regions, but not in the remainder of the filamentary clouds in Ophiuchus.

5.   Conclusions

We have presented the 14.4 square degree c2d *Spitzer* MIPS long wavelength imaging survey of the Ophiuchus molecular cloud complex. Many point sources and a variety of extended emission structures on scales from circumstellar to intercloud are shown in our mosaicked images. Using point-source fitting photometry, we have identified and measured the brightness of 5779 sources at 24 μm, 81 sources at 70 μm, and 8 sources at 160 μm. Using criteria derived from a K_s versus K_s-[24] and other color-color and color-magnitude diagrams, we have identified some 323 candidate young stellar objects throughout the clouds. Several sources with extreme colors are discussed, and a candidate edge-on disk is identified. Our survey suggests that although the numbers of forming stars are dominated by the L1688 cluster and small aggregates in L1689 and L1709, there may be a population of Class II sources lurking in the more tenuous parts of the cloud. This distributed population could contain up to 40% of the YSO candidates in Ophiuchus.

REFERENCES

Allen, L.E., Myers, P.C., Di Francesco, J., Mathieu, R., Chen, H., Young, E. 2002, ApJ, 566, 993

Allen, L.E., Myer, P.C., Di Francesco, J., Mathieu, R., Chen, H., Young, E. 2002, ApJ, 566, 993

[bont]Bontemps, S, et al., 2001, A&A, 372, 173

Barsony, M., Carlstrom, J.E., Burton, M.G., Russell, A.P.G., Garden, R. 1989, ApJ, 346, 93

Barsony, M., Kenyon, S., Lada, E.A., Teuben, P.J. 1997, ApJS, 112, 109

Barsony, M., Ressler, M.E., Marsh, K.A. 2005, ApJ, 630, 381

Beckwith, S.V.W., Sargent, A.I., Chini, R.S., Guesten, R. 1990, AJ, 99, 924

Beichman, C., et al., 1986, ApJ, 307, 337

Beichman, C. A., et al. 1988, IRAS catalog and explanatory supplment

Bontemps, S., Andrè, P., Kaas, A.A., Nordh, L., Olofsson, G., Huldtgren, M., Abergel, A., et al. 2001, A&A, 372, 173

Bontemps, S., Andrè, P., Kaas, A. A., Nordh, L., Olofsson, G., Huldtgren, M., Abergel, A., Blommaert, J., Boulanger, F., Burgdorf, M., et al. 2001, A&A, 372, 173

Bouvier, J., Appenzeller, I. 1992, A&AS, 92, 481

Burrows, C.J., et al. 1996, ApJ, 473, 437

Chapman, N., et al. 2007, ApJ, submitted

Chini, R. 1981, A&A, 99, 346

Comeron, F., Rieke, G.H., Burrows, A., Rieke, M.J. 1993, ApJ, 416, 185

Cushing, M.C., Tokunaga, A.T., Kobayashi, N. 2000, AJ, 119, 3019

Cutri, R. et al. 2003, http://irsa.ipac.caltech.edu/applications/Gator/

Devito, B., Haywood, T.L. 1998, ApJ, 504, 43

de Zeeuw, P.T., Hoogerwerf, R., de Bruijne, J.H.J., Brown, A.G.A., Blaauw, A. 1999, AJ, 117, 354

Dolidze, M. & Arakelian, M. 1959, Astron. Zh., 36, 444

Duchêne, G., Bouvier, J., Bontemps, S., André, P., Motte, F. 2004, A&A, 427, 651

Evans, N.J., II, Allen, L.E., et al. 2003, PASP, 115, 965

Evans, N.J., II, et al. 2006, c2d delivery documents, available online

Grasdalen, G.L., Strom, S.E., Strom, K.M. 1973, ApJ, 184, 53

Gomez, M., Whitney, B.A., Wood, K. 1998, 115, 2018

Greene, T.P., Young, E.T. 1992, ApJ, 395, 516

Greene, T.P., Wilking, B.A., André, P., Young, E.T., Lada, C.J. 1994, ApJ, 434, 614

Greene, T.P., Meyer, M.R. 1995, ApJ, 450, 233

Guglielmo, F., Epchtein, N., Le Bertre, T., Fouque, P., Hron, J., Kerschbaum, F., Lepine, J.R.D. A&AS, 99, 31

Haisch, K.E., Jr., Barsony, M., Greene, T.P., Ressler, M.E. 2002, AJ, 124, 2841

Harvey, P.M., et al. 2006, ApJ, 644, 307

Harvey, P.M., et al. 2007, in preparation

Jørgensen, J.K., et al. 2005, ApJ, 631, L77

Jørgensen, J.K., et al. 2006, ApJ, 645, 1246

Klose, S. 1986, A&SS, 128, 135

Lada, C.J., Wilking, B.A. 1984, ApJ, 287, 610

Lada, C.J., Wilking, B.A., Young, E. 1989, ApJ, 340, 823

Loren, 1989, ApJ, 338, 902

Luhman, K.L., Rieke, G.H. 1999, ApJ, 525, 440

Makovoz, D., Roby, T., Khan, I., Hartley, B. 2006, ProcSPIE, 6274, 62740C

Martín, E.L., Montmerle, T., Gregorio-Hetem, J., Casanova, S. 1998, MNRAS, 300, 733

Moshir, M., Kopman, G., Conrow, T., IRAS Faint Source Survey and Explanatory Supplement

Natta, A., Testi, L., Randich, S. 2006, A&A, 452, 245

Nutter, D., Ward-Thompson, D., André, P. 2006, MNRAS, 368, 1833

Phelps, R.L., Barsony, M. 2004, ApJ, 127, 420

Porras, A., et al. 2007, ApJ, 656, 493

Rebull, L., et al. 2007, ApJS, 171, 447

Ressler, M. and Barsony, M. 2003, Ap.J., 584, 832

Ridge, N., et al. 2006, AJ, 131, 2921

Rieke, G.H., Ashok, N.M., Boyle, R.P. 1989, ApJ, 339, 71

Robitaille, T.P., Whitney, B.A., Indebetouw, R., Wood, K., Denzmore, P. 2006, ApJ, 167, 256

Shupe, D., et al. 2006, ApJ, in press

Spiesman, W., et al. 2006, in preparation

Stanke, et al., 2006, A&A, 447, 609

Strom, K.M., Kepner, J., Strom, S.E. 1995, ApJ, 438, 813

Stapelfeldt, K.R. et al. 2006, BAAS/DPS, 38, 58.06

Visser, A.E., Richer, J.S., Chandler, C.J. 2002, AJ, 124, 2756

Vrba, F.J., Strom, K.M., Strom, S.E., Grasdalen, G.L. 1975, ApJ, 197, 77

Wainscoat, R. J., Cowie, L.L. 1992, AJ, 103, 332

Wilking, B.A., Lada, C.J. 1983, ApJ, 274, 698

Wilking, B.A., Lada, C.J., Young, E.T. 1989, ApJ, 340, 823

Wilking, B.A., Greene, T.P., Meyer, M.R. 1999, AJ, 117, 469

Wilking, B.A., Meyer, M.R., Robinson, J.G., Greene, T.P. 2005, AJ, 130, 1733

Wood, K., Lada, C.J., Bjorkman, J.E., Kenyon, S.J., Whitney, B., Wolff, M.J. 2002, ApJ, 567, 1183

Young, E.T., et al. 2004, ApJS, 154, 428

Young, K.E., et al. 2005, ApJ, 628, 283

Young, K.E., et al. 2006, ApJ, 644, 326

Table 1.   Summary of observations (Program 177)

field	map center	first epoch AORKEY	second epoch AORKEY
ophi-mips1	16h45m50.0s,-21d21m16.0s	5745408	5747200
ophi-mips2	16h43m24.0s,-21d57m38.0s	5745664	5747456
1689-mips1	16h43m16.0s,-24d09m09.4s	5748992	5753344
1689-mips2	16h38m27.0s,-24d18m02.0s	5749248	5753600
1689-mips3	16h35m12.0s,-24d34m00.0s	5749504	5753856
1688-mips1	16h33m33.0s,-24d20m42.0s	5757952	5766144
1688-mips2	16h33m01.5s,-23d18m20.0s	5758208	5766400
1688-mips3	16h31m59.2s,-24d57m53.0s	5758464	5766656
1688-mips4	16h31m00.0s,-23d37m50.1s	5758720	5766912
1688-mips5	16h30m03.0s,-25d08m22.0s	6605568	6605824
1688-mips6	16h27m56.5s,-24d11m12.0s	5759488	5767680
1688-mips7	16h25m46.0s,-24d12m29.0s	5759744	5676936
1688-mips8	16h24m09.0s,-23d50m03.0s	5760000	5768192
1688-mips9	16h21m52.5s,-23d43m45.0s	5760256	5768448
oph-oc7	16h23m52.0s,-21d57m38.0s	5778432	5778688
oph-oc8	16h23m12.0s,-26d28m49.0s	5778944	5779200

Table 2.   Box regions used to define individual clouds

cluster	α, δ of box corners
L1688	16 30 12.0 -24 49 15.6, 16 25 05.5 -23 49 15.6
L1689	16 35 33.6 -25 30 00.0, 16 31 10.6 -24 10 37.2
L1709	16 35 33.6 -24 10 37.2, 16 30 12.0 -23 20 45.6
L1712 + L1729	16 46 28.1 -24 46 58.8, 16 35 33.6 -23 42 07.2
North	16 48 10.3 -22 09 03.6, 16 42 21.6 -20 50 34.8

Table 3.   Detected Sources

item	overall	in IRAC cvg	L1688	L1689	L1709	L1712+L1729	rest of cloud	North	off-cloud
number 24 μm objects	5779	2608	569	490	377	1082	2555	706	355
number 70 μm objects	81	31	24	12	5	12	14	13	2
number 160 μm objects	8	6	1	1	2	1	1	2	0
number 24&70 objects	50	31	13	6	4	5	11	11	0
number 24&70&160 objects	5	4	1	1	1	1	0	1	0
number 24 μm & K objects	2590	1197	297	195	149	539	1102	308	177
number 24 μm & any IRAC objects	2306	2306	425	351	144	379	895	112	0
number 70 μm & any IRAC objects	42	30	23	7	4	3	4	1	0
number 160 μm & any IRAC objects	6	6	1	1	2	1	0	1	0

Table 4.　Classification based on $K_\mathrm{s}-[24]$

item	entire cloud	L1688	L1689	L1709	L1712+L1729	rest of cloud	North	off-cloud
number objects with K_s and 24 μm	2590	297	195	149	539	1102	308	177
number with $K_\mathrm{s}-[24]>2$, $K_\mathrm{s}<14$	323	161	27	13	18	96	8	2
number with $K_\mathrm{s}-[24]>2$, $K_\mathrm{s}<14$, and Class I $K_\mathrm{s}-[24]$ color	20 (6%)	12 (7%)	2 (7%)	1 (7%)	0 (0%)	5 (5%)	0	0
number with $K_\mathrm{s}-[24]>2$, $K_\mathrm{s}<14$, and "flat" $K_\mathrm{s}-[24]$ color	47 (14%)	33 (20%)	3 (11%)	4 (30%)	1 (5%)	5 (5%)	1 (12%)	0
number with $K_\mathrm{s}-[24]>2$, $K_\mathrm{s}<14$, and Class II $K_\mathrm{s}-[24]$ color	207 (64%)	100 (62%)	20 (74%)	7 (53%)	5 (27%)	73 (76%)	2 (25%)	1 (50%)
number with $K_\mathrm{s}-[24]>2$, $K_\mathrm{s}<14$, and Class III $K_\mathrm{s}-[24]$ color	49 (15%)	16 (9%)	2 (7%)	1 (7%)	12 (66%)	13 (13%)	5 (62%)	1 (50%)

Table 5.   IRAS Results in MIPS Ophiuchus Map (main+North)

item	… at 24	… at 70 μm
12 μm PSC real (IRAS qual=3) detections	100	91
cleanly retrieved	74 (74%)	25 (27%)
completely missing	2 (2%)	41 (45%)
nebulosity; no point source	15 (15%)	24 (26%)
resolved as multiple	9 (9%)	1 (1%)
25 μm PSC real (IRAS qual=3) detections	63	63
cleanly retrieved	41 (65%)	26 (41%)
completely missing	1 (1%)	12 (19%)
nebulosity; no point source	15 (23%)	24 (38%)
resolved as multiple	6 (9%)	1 (1%)
60 μm PSC real (IRAS qual=3) detections	93	84
cleanly retrieved	23 (24%)	20 (23%)
completely missing	41 (44%)	16 (19%)
nebulosity; no point source	27 (29%)	48 (57%)
resolved as multiple	2 (2%)	0 (0%)
100 μm PSC real (IRAS qual=3) detections	55	50
cleanly retrieved	4 (7%)	3 (6%)
completely missing	29 (52%)	12 (24%)
nebulosity; no point source	22 (40%)	35 (70%)
resolved as multiple	0 (0%)	0 (0%)
12 μm FSC real (IRAS qual=3) detections	50	35
cleanly retrieved	42 (84%)	3 (8%)
completely missing	0 (0%)	24 (68%)
nebulosity; no point source	7 (14%)	8 (22%)
resolved as multiple	1 (2%)	0 (0%)
25 μm FSC real (IRAS qual=3) detections	14	11
cleanly retrieved	13 (92%)	5 (45%)
completely missing	0 (0%)	6 (54%)
nebulosity; no point source	0 (0%)	0 (0%)
resolved as multiple	1 (7%)	0 (0%)
60 μm FSC real (IRAS qual=3) detections	0	0

Table 5—Continued

item	... at 24	... at 70 μm
100 μm FSC real (IRAS qual=3) detections	0	0

Table 6.   IRAS PSC detections not recovered by Spitzer/MIPS

PSC name	. . . from 24 μm	. . . from 70 μm
16169-2443	missing (upper limit at 12,25)	missing (det@60, upp lim@100)
16172-2503	missing (upper limit at 12,15)	confused by nebulosity
16173-2422	confused by nebulosity	missing (det@60, upp lim@100)
16184-2452	confused by nebulosity	confused by nebulosity
16184-2452	confused by nebulosity	confused by nebulosity
16187-2339	confused by nebulosity	missing (upper limit at 60,100)
16193-2335	confused by nebulosity	confused by nebulosity
16193-2401	confused by nebulosity	confused by nebulosity
16193-2450	confused by nebulosity	confused by nebulosity
16194-2410	missing (upper limit at 12,25)	confused by nebulosity
16194-2500	off edge	confused by nebulosity
16196-2443	missing (upper limit at 12,25)	confused by nebulosity
16200-2251	confused by nebulosity	confused by nebulosity
16201-2410	retrieved (upper limit at 12)	confused by nebulosity
16202-2356	missing (upper limit at 12,25)	confused by nebulosity
16202-2427	missing (upper limit at 12,25)	missing (det@60, upp lim@100)
16203-2332	missing (upper limit at 12,25)	missing (det@60, upp lim@100)
16205-2308	missing (upper limit at 12,25)	confused by nebulosity
16209-2422	confused by nebulosity	confused by nebulosity
16212-2316	missing (upper limit at 12,25)	missing (det@60, upp lim@100)
16214-2302	missing (upper limit at 12,25)	confused by nebulosity
16214-2345	confused by nebulosity	confused by nebulosity
16214-2436	confused by nebulosity	confused by nebulosity
16217-2244	missing (upper limit at 12,25)	confused by nebulosity
16219-2344	confused by nebulosity	confused by nebulosity
16219-2417	confused by nebulosity	confused by nebulosity
16221-2428	confused by nebulosity	confused by nebulosity
16222-2358	confused by nebulosity	confused by nebulosity
16223-2404	confused by nebulosity	confused by nebulosity
16225-2417	confused by nebulosity	confused by nebulosity
16226-2319	broken into pieces	confused by nebulosity

Table 6—Continued

PSC name	. . . from 24 μm	. . . from 70 μm
16226-2420	confused by nebulosity	confused by nebulosity
16227-2418	confused by nebulosity	confused by nebulosity
16228-2432	confused by nebulosity	confused by nebulosity
16229-2413	confused by nebulosity	confused by nebulosity
16233-2421	confused by nebulosity	confused by nebulosity
16234-2436	confused by nebulosity	confused by nebulosity
16234-2436	confused by nebulosity	confused by nebulosity
16235-2416	retrieved	confused by nebulosity
16238-2317	missing (upper limit at 12,25)	confused by nebulosity
16246-2440	retrieved	confused by nebulosity
16257-2533	missing (upper limit at 12,25)	confused by nebulosity
16262-2545	retrieved	missing (det@60, upp lim@100)
16265-2350	missing (upper limit at 12,25)	confused by nebulosity
16267-2539	confused by nebulosity	confused by nebulosity
16268-2533	missing (upper limit at 12,25)	missing (det@60, upp lim@100)
16269-2454	confused by nebulosity	confused by nebulosity
16272-2541	confused by nebulosity	confused by nebulosity
16274-2349	confused by nebulosity	confused by nebulosity
16275-2251	missing (upper limit at 12,25)	missing (det@60, upp lim@100)
16277-2356	confused by nebulosity	missing (det@60, upp lim@100)
16280-2353	confused by nebulosity	missing (det@60, upp lim@100)
16281-2514	missing (upper limit at 12,25)	confused by nebulosity
16285-2519	missing (upper limit at 12,25)	confused by nebulosity
16289-2527	missing (upper limit at 12,25)	confused by nebulosity
16301-2525	missing (upper limit at 12,25)	confused by nebulosity
16303-2428	confused by nebulosity	confused by nebulosity
16304-2504	missing (upper limit at 12,25)	confused by nebulosity
16306-2435	confused by nebulosity	confused by nebulosity
16311-2419	confused by nebulosity	confused by nebulosity
16313-2439	confused by nebulosity	confused by nebulosity
16318-2519	missing (upper limit at 12,25)	missing (det@60, upp lim@100)

Table 6—Continued

PSC name	. . . from 24 μm	. . . from 70 μm
16322-2421	confused by nebulosity	confused by nebulosity
16325-2433	confused by nebulosity	confused by nebulosity
16330-2424	missing (upper limit at 12,25)	confused by nebulosity
16330-2431	missing (upper limit at 12,25)	confused by nebulosity
16335-2402	missing (upper limit at 12,25)	missing (det@60, upp lim@100)
16335-2419	missing (upper limit at 12,25)	confused by nebulosity
16339-2422	missing (upper limit at 12,25)	confused by nebulosity
16341-2413	missing (upper limit at 12,25)	missing (det@60, upp lim@100)
16342-2413	missing (upper limit at 12,25)	missing (det@60, upp lim@100)
16375-2439	missing (upper limit at 12,25)	confused by nebulosity
16379-2444	missing (upper limit at 12,25)	missing (det@60, upp lim@100)
16383-2407	missing (upp lim@12, det@25)	missing (upper limit at 60,100)
16414-2337	missing (upper limit at 12,25)	missing (det@60, upp lim@100)
16417-2155	confused by nebulosity	confused by nebulosity
16418-2155	confused by nebulosity	confused by nebulosity
16421-2146	confused by nebulosity	confused by nebulosity
16426-2129	confused by nebulosity	confused by nebulosity
16436-2121	confused by nebulosity	confused by nebulosity

Table 7.   MIPS photometry for point-source objects discussed in this paper

SSTc2d name	region	MIPS-24 (mJy)[a]	MIPS-70 (mJy)[a]	MIPS-160 (mJy)[a]	other names[b]	notes
				Red sources selected by a variety of means (see text)		
162145.1-234231	rest of cloud	206	730	...	[L89] R7	
162218.5-232148	rest of cloud	804	770	...	IRAS 16193-2314=WSB 12	
162309.2-241704	rest of cloud	715	1400	...	IRAS 16201-2410	
162502.0-245932	rest of cloud	395	630	...	IRAS 16220-2452=WSB 19	
162510.5-231914	rest of cloud	840	860	...	IRAS 16221-2312=V2503 Oph=DoAr 16=WSB 20=HBC 257	
162524.3-242756	L1688	127	...	...	HD 147889	discussed in §4.1.1
162623.5-242439	L1688	927	...	...	CRBR 2322.1-1754 (=possibly ISO-Oph 37)	discussed in §4.1.1
162646.4-241200	L1688	287	250	...	YLW 37	
162648.4-242838	L1688	455	...	...	CRBR 2346.8-2157 (=possibly ISO-Oph 70=WL 2)	discussed in §4.1.1
162706.7-243814	L1688	2710	3600	...	BBRCG 22=ISO-Oph 103=WL 17	
162713.8-244331	L1688	318	550	...	ISO-Oph 117=WLY 2-32b	
162717.5-242856	L1688	855	...	...	ISO-Oph 124=YLW 12A	discussed in §4.1.1
162737.2-244238	L1688	576	890	...	(=possibly ISO-Oph 161 - 6″ away)	discussed in §4.1.1
162738.3-243658	L1688	702	930	...	IRAS 16246-2430=ISO-Oph 163=WLY 1-47=WLY 2-49	
162738.9-244020	L1688	474	1200	...	ISO-Oph 165	
162739.4-243915	L1688	1160	1400	...	ISO-Oph 166=WSB 52	
162739.8-244315	L1688	2520	2900	...	IRAS 16246-2436=ISO-Oph 167=WLY 2-51=WLY 1-45	
162741.6-244644	L1688	72	320	...	ISO-Oph 170	
162816.5-243657	L1688	239	620	...	(=possibly ISO-Oph 196=WSB 60 - 8″ away)	
162821.6-243623	L1688	94	2100	9910	[SSG2006] MMS126	
162845.2-242819	L1688	737	1100	...	V853 Oph=DoAr 40=IRAS 16257-2421=ISO-Oph 199=WSB 62	
162857.8-244054	L1688	167	240	...	(=possibly BKLT J162858-244054 - 7″ away)	
163130.8-242439	L1689	1250	900	4690	IRAS 16284-2418=DoAr 43=WSB 71	
163133.4-242737	L1689	1430	2600	...	IRAS 16285-2421=DoAr 44=SVS 2114=HBC 268=WSB 72	
163133.8-240446	L1709	717	440	...	IRAS 16285-2358	
163135.6-240129	L1709	2980	10647	19000	IRAS 16285-2355=WLY 2-63	
163136.7-240420	L1709	194	670	...	...	
163143.7-245524	L1689	1210	1400	...	ISO-Oph 200	
163144.5-240212	L1709	275	390	...	...	
163152.4-245536	L1689	887	680	...	ISO-Oph 203	
163154.7-250323	L1689	1380	1400	...	WSB 74 (=possibly IRAS 16289-2457)	
163222.6-242832	L1689	595	...	...	IRAS 16293-2422	discussed in §4.1.1

Table 7—Continued

SSTc2d name	region	MIPS-24 (mJy)[a]	MIPS-70 (mJy)[a]	MIPS-160 (mJy)[a]	other names[b]	notes
163355.6-244204	L1689	235	740	...	RX J1633.9-2442=[NWA2006] SMM17	
163528.6-245648	L1689	...	740.0	...	CD-24 12715	debris disk candidate; see §4.1.1
163945.4-240203	L1712+L1729	1420	2000	4560	IRAS 16367-2356=WSB 82	
164417.8-220648	north	1240	220	...	IRAS 16413-2201	debris disk candidate; see §4.1.1
164526.1-250316	rest of cloud	150	260	...	IRAS 16424-2457	
			L1709 aggregate			
163129.2-240431	L1709	82.2	...	...		src 1 in §4.1.2
163133.8-240446	L1709	717.0	440.0	...	IRAS 16285-2358	src 2 in §4.1.2
163134.2-240325	L1709	747.0	...	18300.0		src 3 in §4.1.2
163135.6-240129	L1709	2980.0	10647.0	19000.0	IRAS 16285-2355	src 4 in §4.1.2
163136.7-240420	L1709	194.0	670.0	...		src 5 in §4.1.2, new edge-on disk candidate
163144.5-240212	L1709	275.0	390.0	...		src 6 in §4.1.2
			L1689 aggregate			
163143.7-245559	L1689	19.9	...	...		src 1 in §4.1.3
163143.7-245524	L1689	1210.0	1400.0	...	ISO-Oph 200	src 2 in §4.1.3
163148.9-245429	L1689	20.9	...	...	ISO-Oph 201	src 3 in §4.1.3
163151.9-245623	L1689	...	1500.0	...	(=possibly ISO-oph 204=LDN 1689 IRS 5)	src 4 in §4.1.3; saturated in nearly all bands
163152.0-245725	L1689	39.8	...	...		src 5 in §4.1.3; unresolved binary
163152.4-245536	L1689	887.0	680.0	...	ISO-Oph 203	src 6 in §4.1.3
163153.4-245505	L1689	104.0	...	...	ISO-Oph 205	src 7 in §4.1.3
163159.3-245440	L1689	43.8	...	...	ISO-Oph 208	src 8 in §4.1.3
163200.9-245641	L1689	...	46800.0	...	IRAS 16289-2450=LDN 1689S	src 9 in §4.1.3

[a]Absolute uncertainties on the 24 μm data are estimated to be 10-15%; statistical uncertainties are much less than this. Uncertainties on 70 and 160 μm flux densities are estimated to be 20%.

[b]Source associations taken from SIMBAD up to 5″ away from Spitzer position (known to a fraction of an arcsecond); possible associations listed in SIMBAD as being 5-8″ away are listed as such. In some cases, there are more than a dozen names for these objects, so only the most common are listed. References for these catalogued sources include Loren (1989; L89), Wilking et al. (2005; WSB), Barsony et al. (1989; BBRCG), Wilking et al. (1989; WLY), Stanke et al. (2006; SSG2006), Barsony et al. (1997; BKLT), Nutter et al. (2006; NWA2006), Dolidze and Arakelian (1959; DoAr), and Bontemps et al. (2001; ISO-Oph).
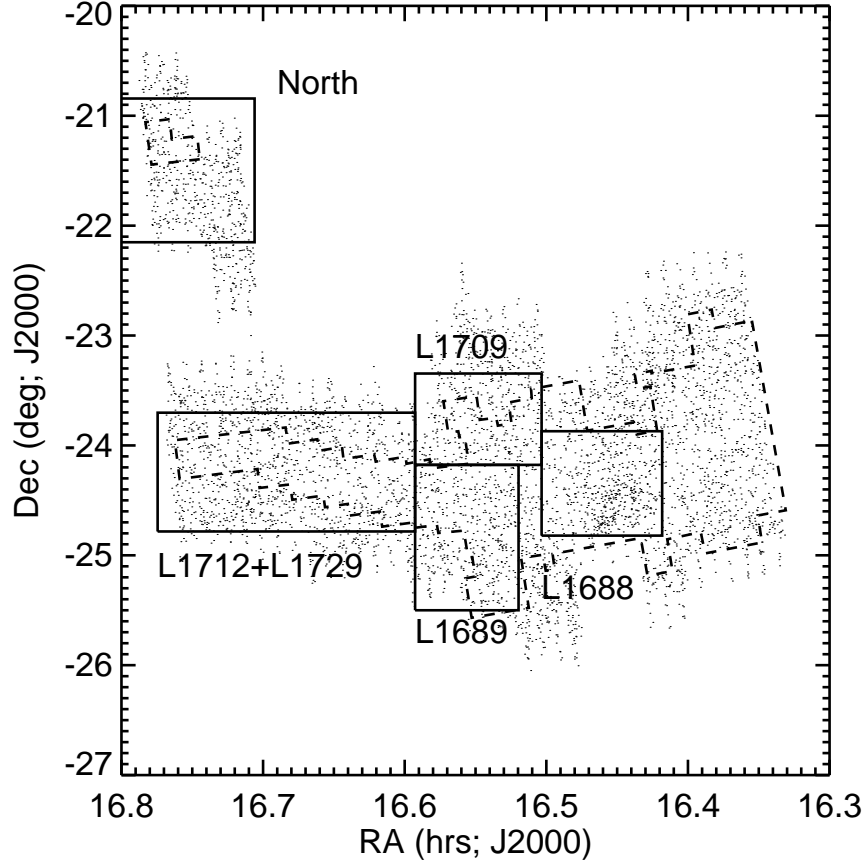
Fig. 1.— Location of MIPS coverage (points are MIPS-24 detections), with the region of IRAC coverage (dashed line) indicated. The smaller squares (solid line) indicates the regions defined to be L1688, L1689, and Ophiuchus North.
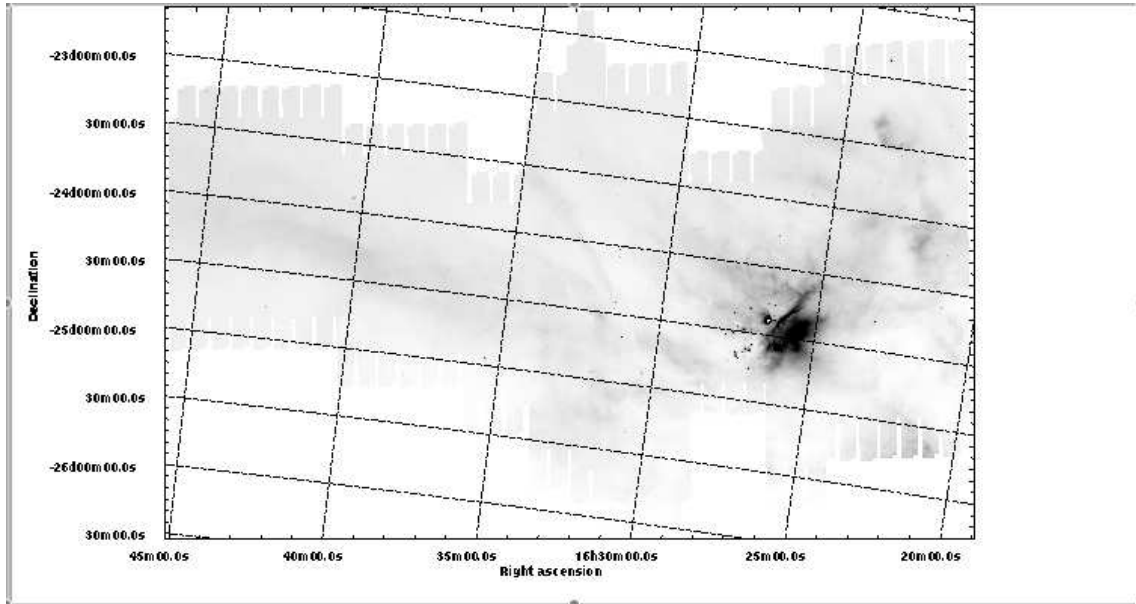
Fig. 2.— *Spitzer* MIPS 24 μm mosaic of Ophiuchus clouds.
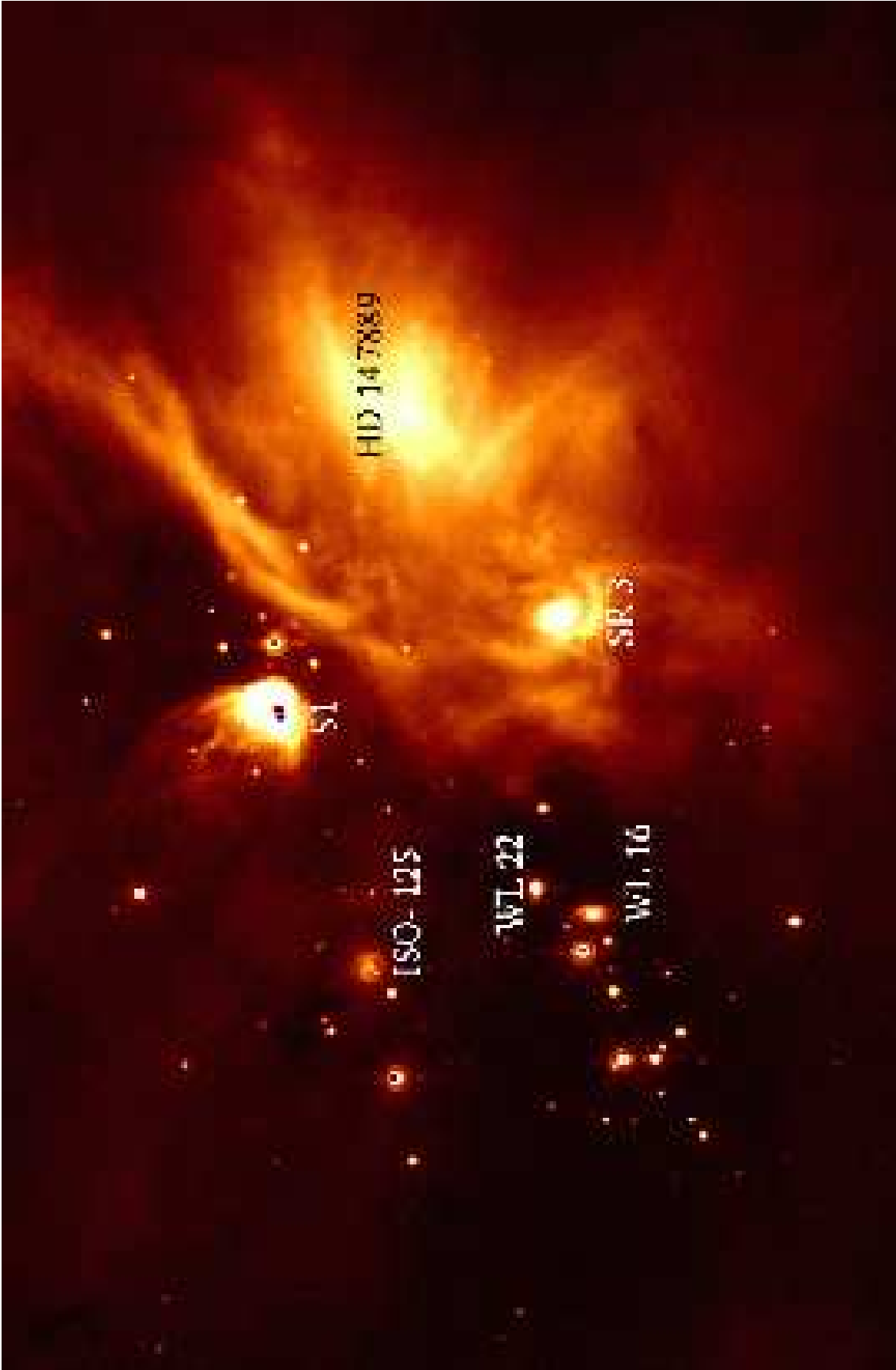
Fig. 3.— MIPS 24 micron image central 1° x 0.5° region region of Lynds 1688.

Fig. 4.— 24 μm dark clouds found near $16^h28^m31^s$-$24°18'$ $40''$. The image spans $15'$ $\times10'$, with N up and E to the left
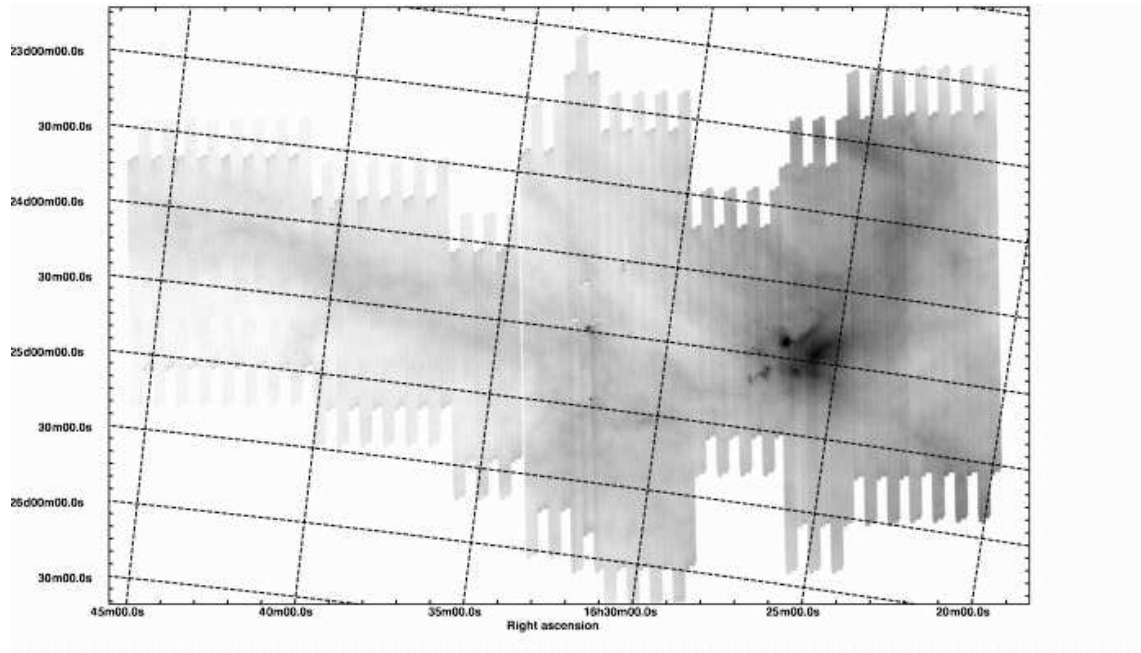
Fig. 5.— *Spitzer* MIPS 70 μm mosaic of Ophiuchus clouds.
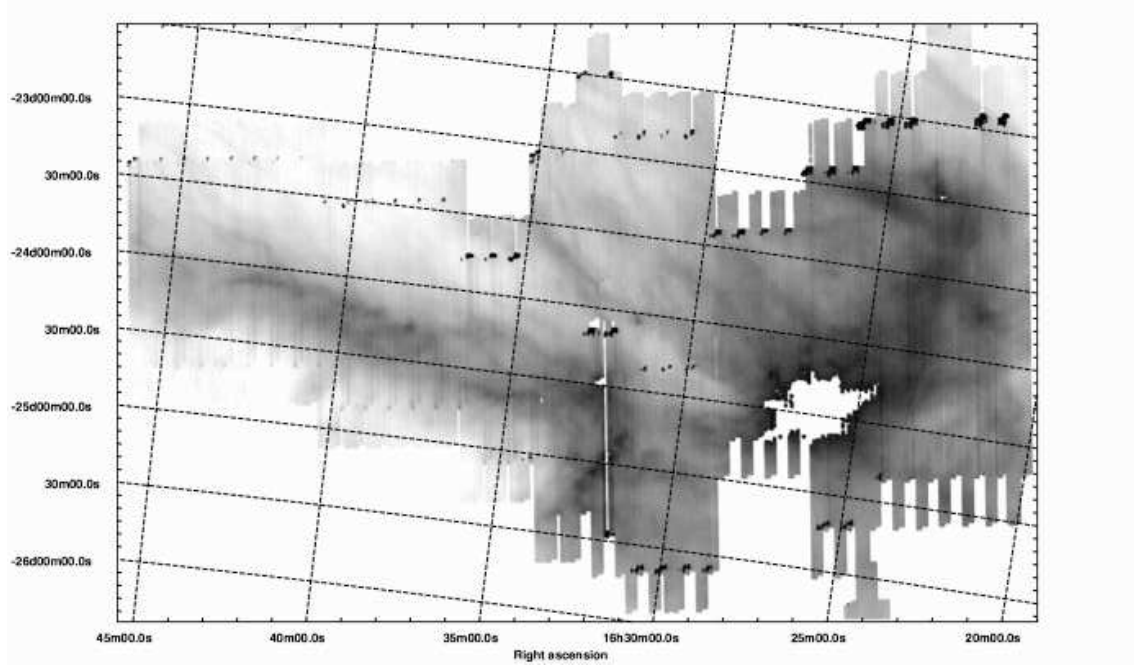
Fig. 6.— *Spitzer* MIPS 160 μm mosaic of Ophiuchus clouds. The central region of the cloud is saturated in our maps.
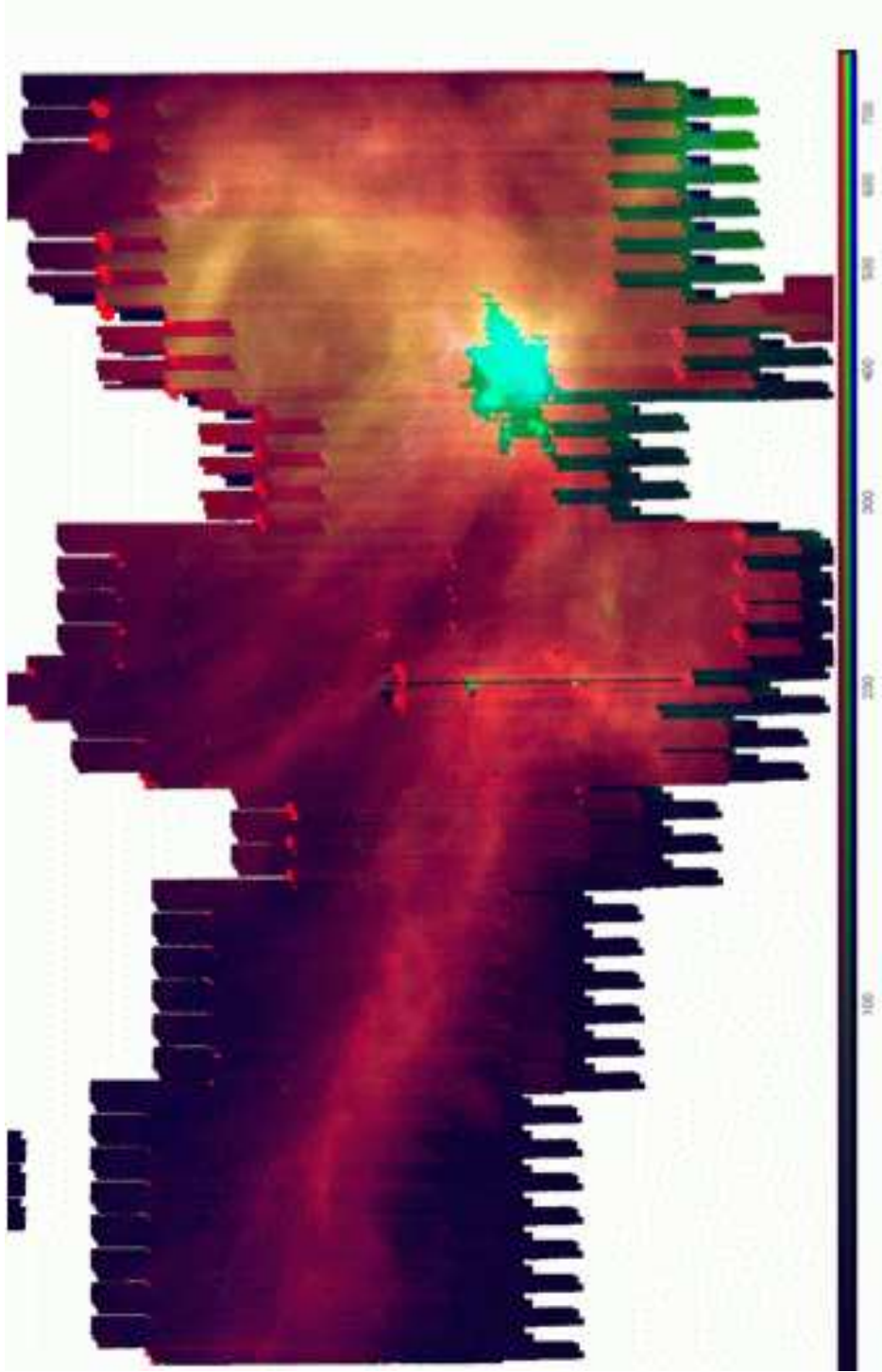
Fig. 7.— 24 (blue), 70 (green), and 160 μm (red) mosaic of Ophiuchus clouds.
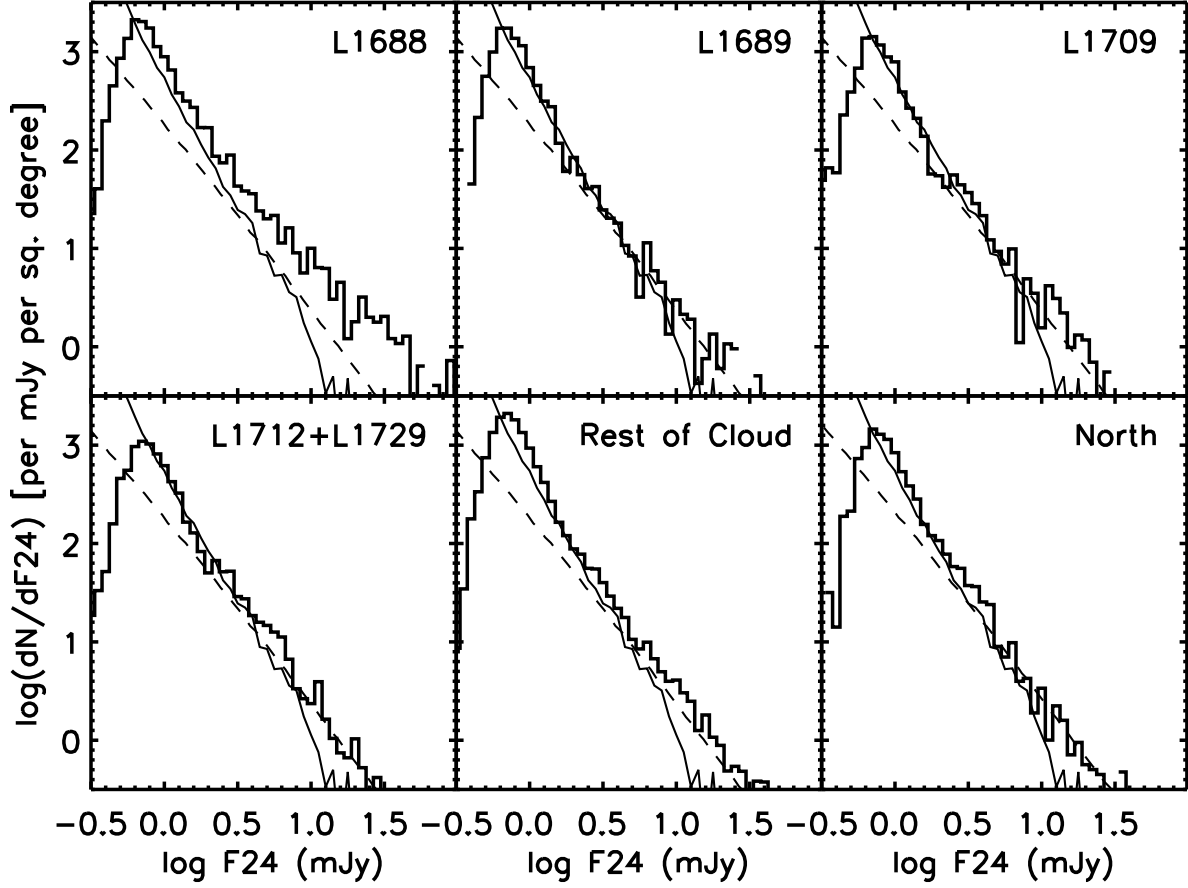
Fig. 8.— Ophiuchus differential number counts at 24 μm. The solid line shows the SWIRE ELAIS N1 extragalactic number counts; the dashed line shows the Wainscoat model prediction of Galactic star counts.
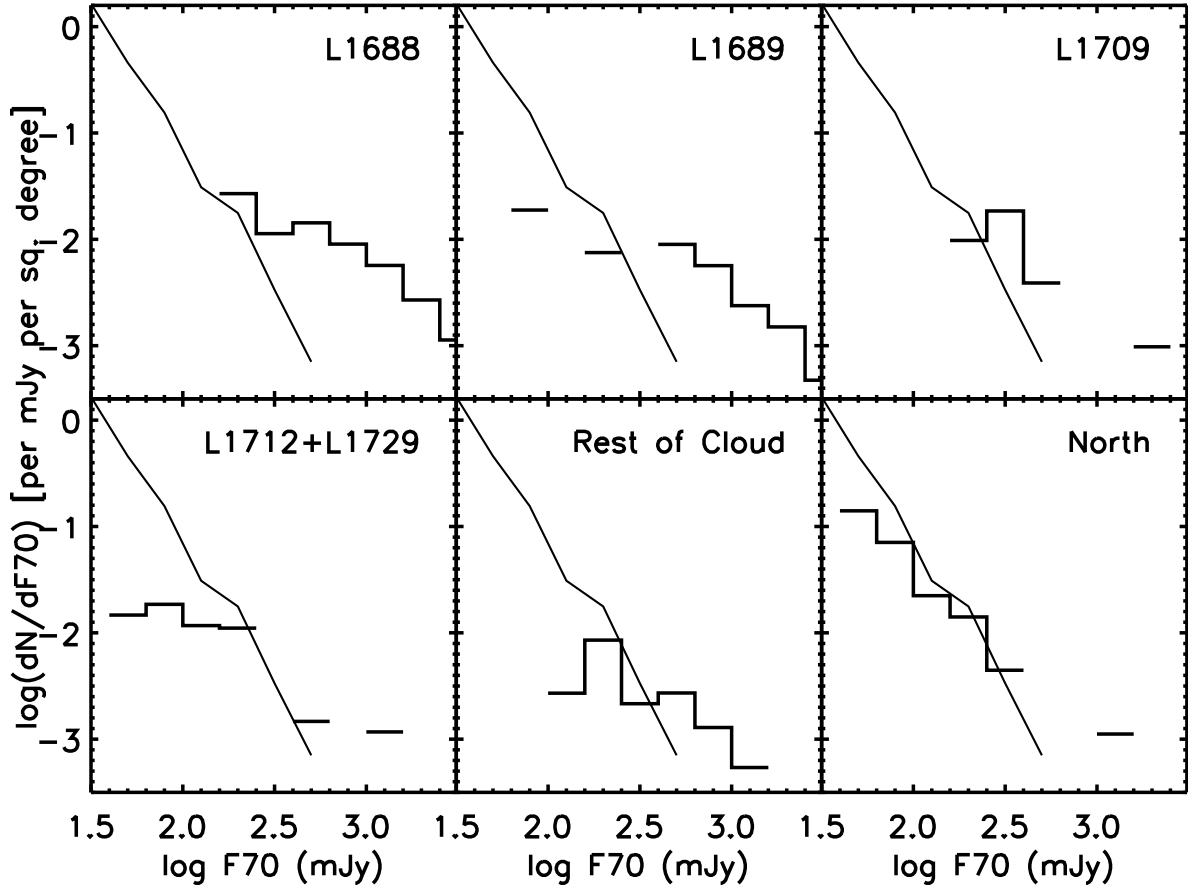
Fig. 9.— Ophiuchus differential number counts at 70 μm. The solid line shows the SWIRE ELAIS N1 extragalactic number counts.
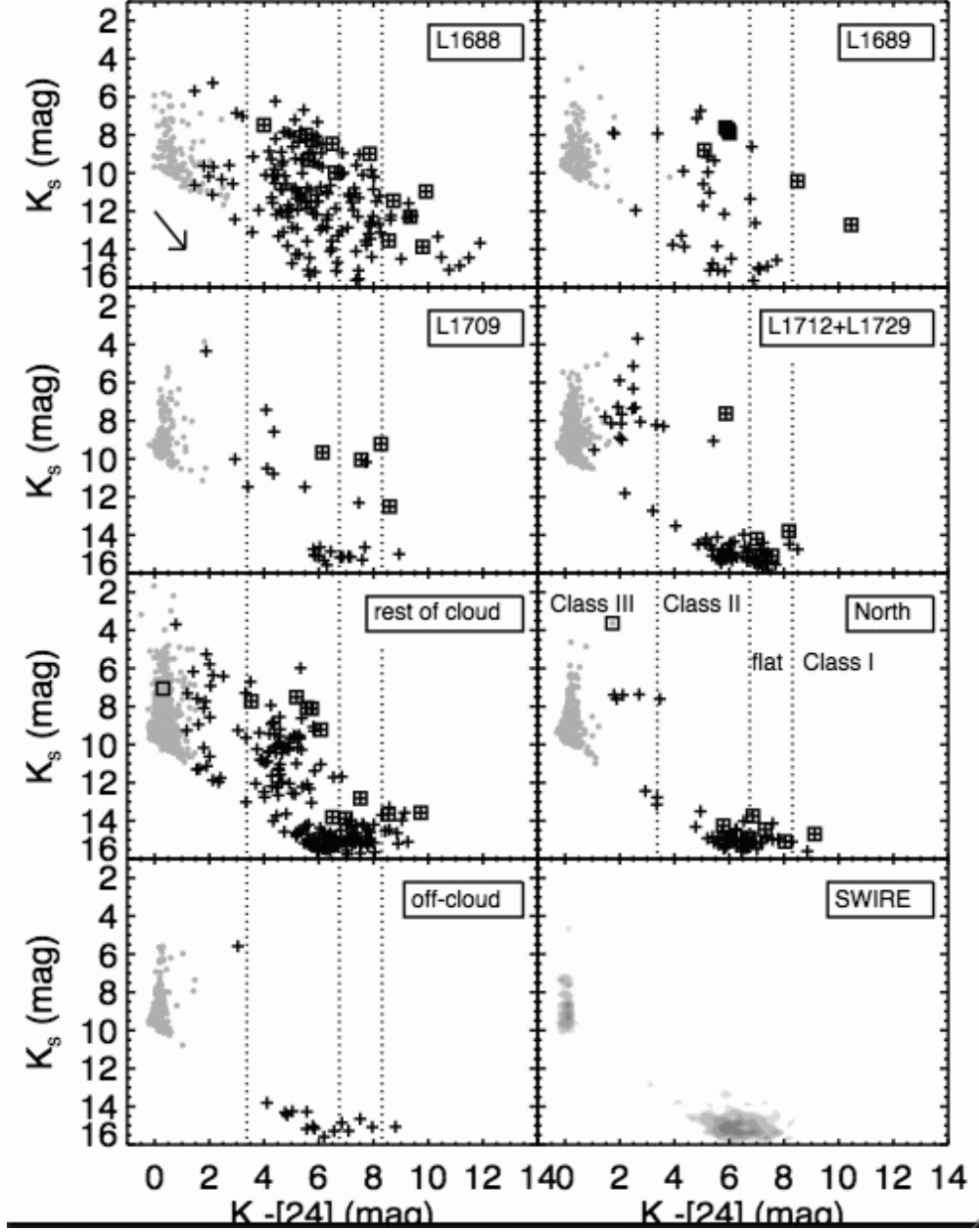
Fig. 10.— K_s vs. $K_s − [24]$ for Ophiuchus objects in the various sub-clusters, as marked, the "rest of the cloud", the off-cloud region, and SWIRE (contour plot, lower right). Objects in SWIRE are expected to be mostly galaxies (objects with $K_s \gtrsim 14$) or plain photospheres (objects with $K_s − [24] \lesssim 1$; marked as grey on the Oph region plots). Boxed sources are also detected at 70 μm. The vertical dashed lines delineate (from left to right) regions where Class I, flat-spectrum, Class II, and Class III infrared source models would reside.
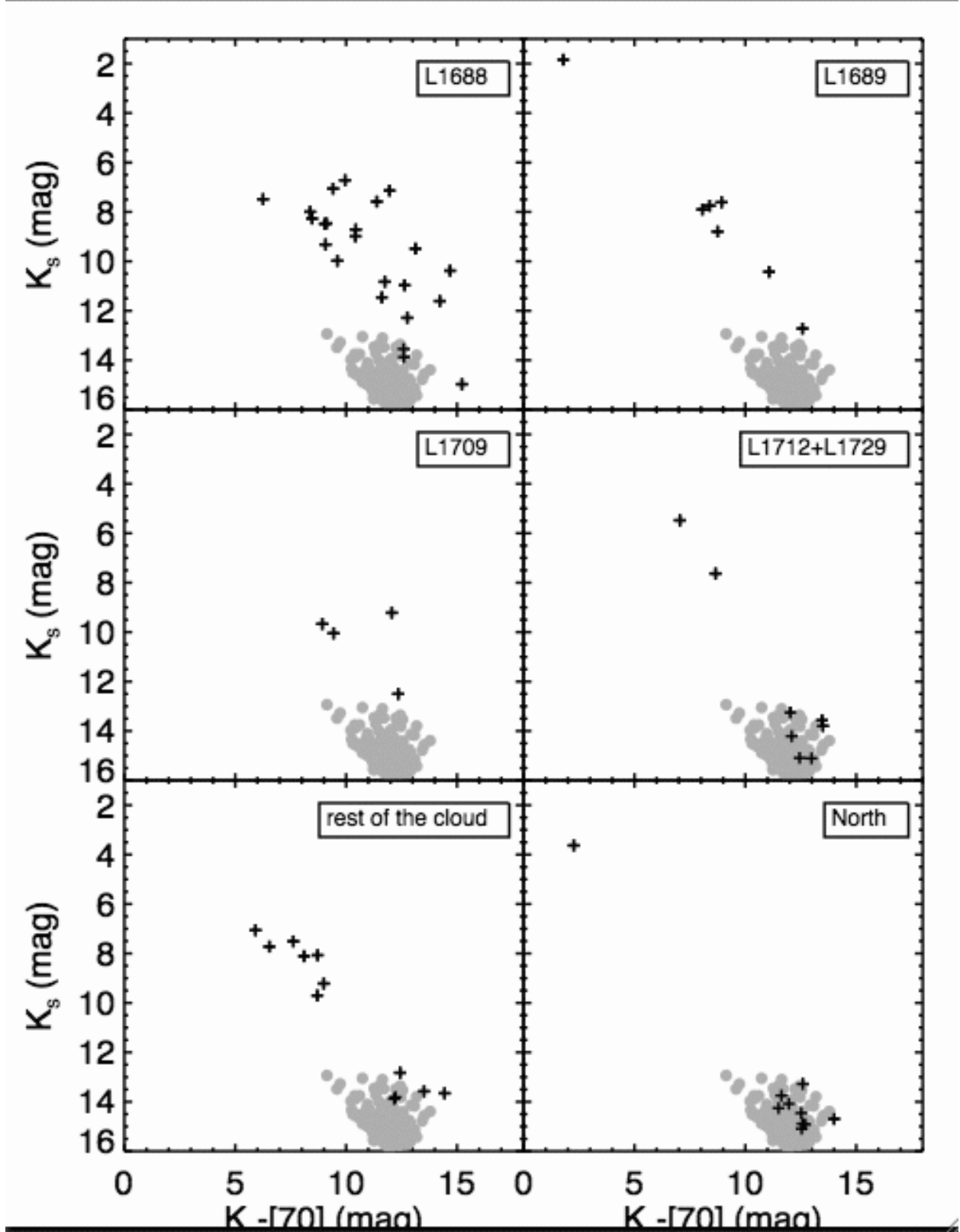
Fig. 11.— K_s vs. $K_s - [70]$ color-magnitude diagram for various regions in Oph (crosses), with data for SWIRE (grey dots) included for comparison. See text for details.
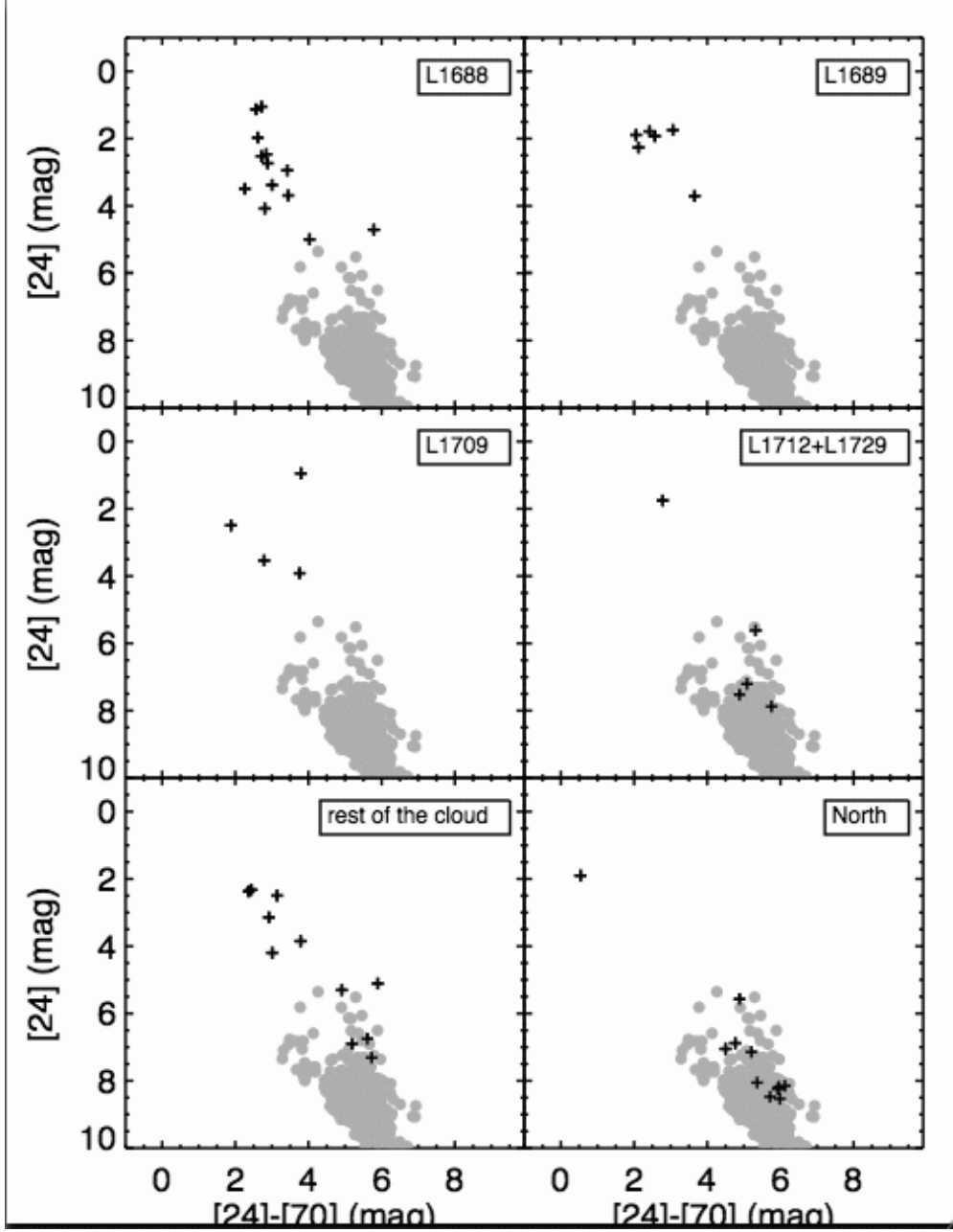
Fig. 12.— [24] vs. [24]−[70] color-magnitude diagram for Ophiuchus (crosses), with data for SWIRE (grey dots) included for comparison. As in Figure 11, the two clumps correspond to extragalactic ([24]∼7-10) and YSO candidates ([24]≲5), and there are few extragalactic objects in the clusters because the high nebulosity limits the depth of the survey. Very red sources ([24]−[70]>6) are the most embedded objects.
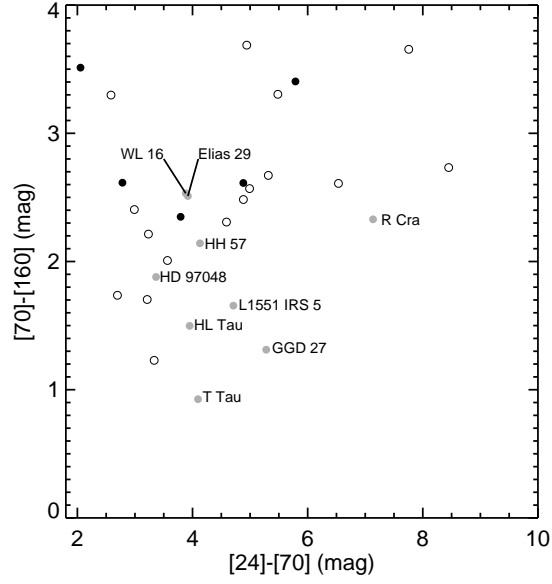
Fig. 13.— Color-color diagram for sources detected but not saturated in all three MIPS bands. Objects shown are from the current Ophiuchus survey (filled circles), the c2d MIPS Perseus survey (open circles; Rebull et al. 2007), and bright objects studied by ISO (grey dots, Noriega-Crespo 2005, private communication).
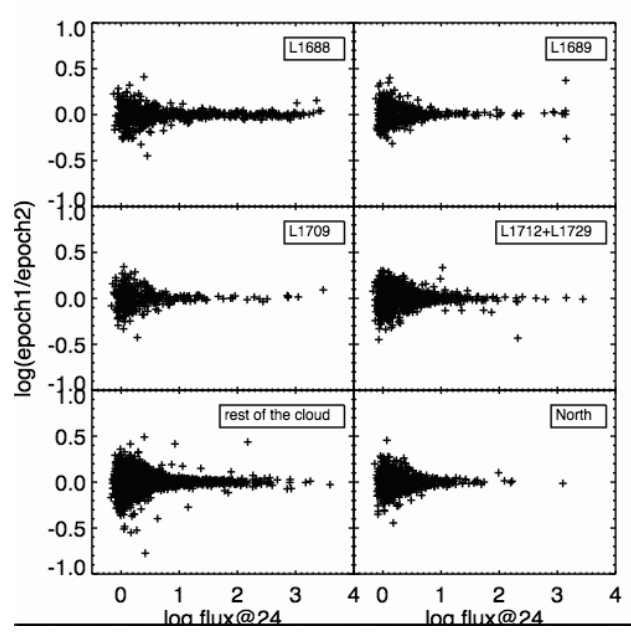
Fig. 14.— Variability of Ophiuchus 24 μm sources between two observations separated by 3 – 8 hours. All cases of potential variability are well explained by instrumental effects
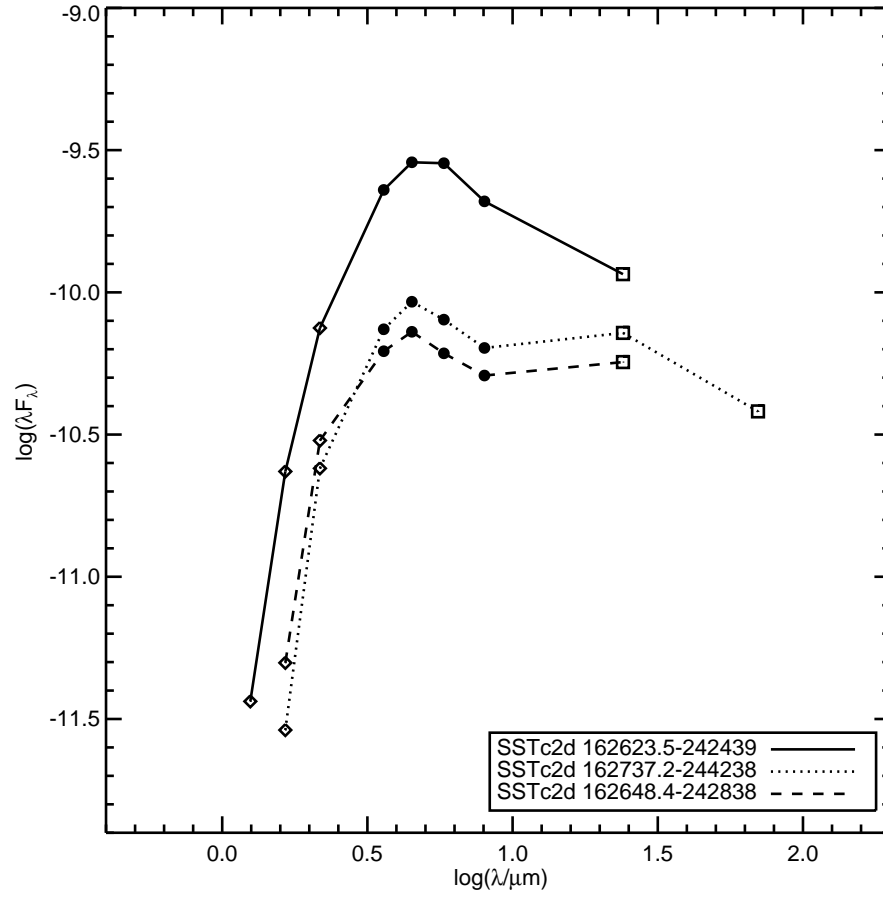
Fig. 15.— Infrared spectral energy distributions of several MIPS sources with $K_s-[24] > 8$.
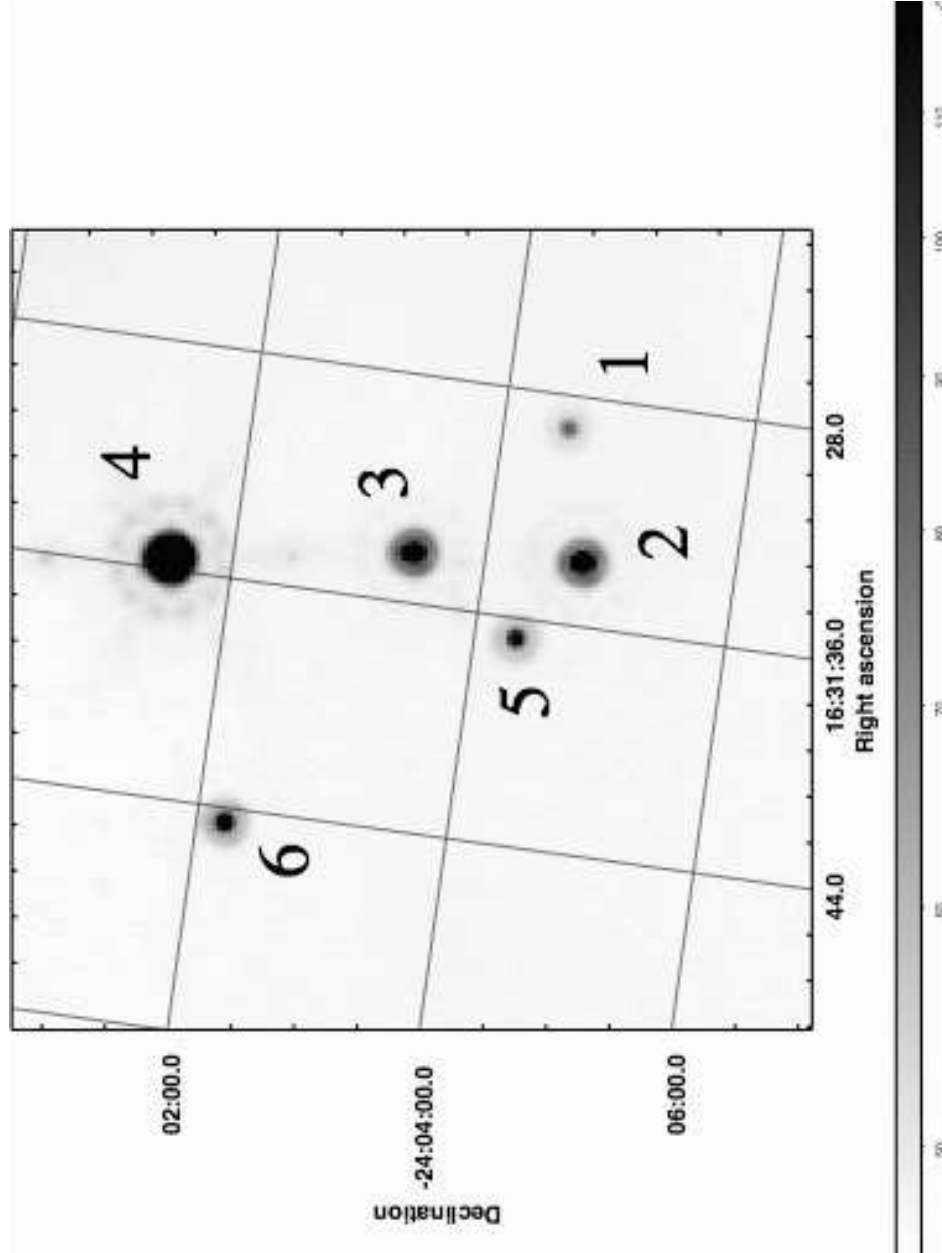
Fig. 16.— 24 μm image and finder chart for the L1709 aggregate.
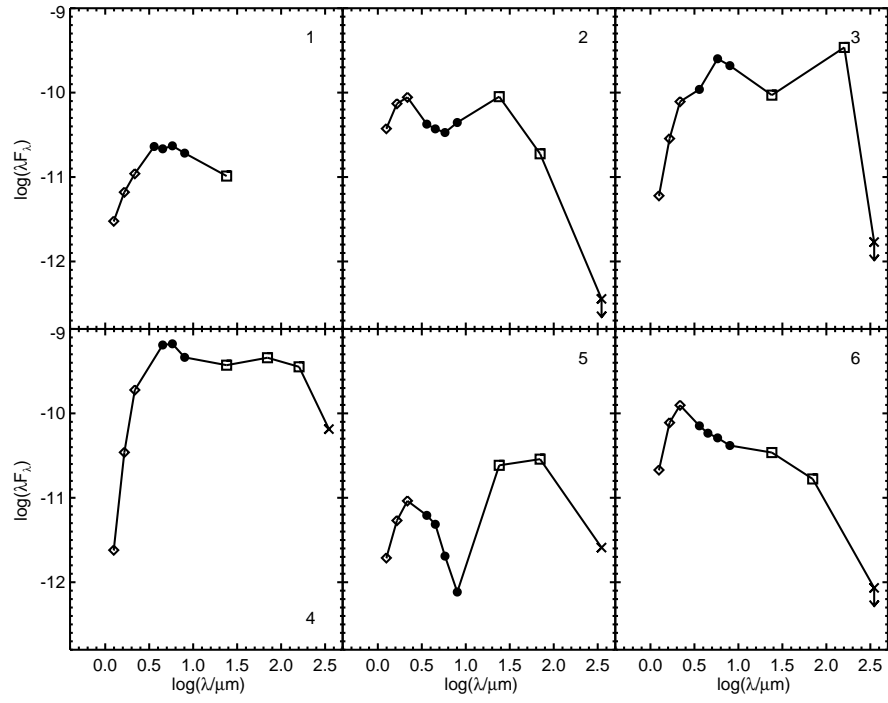
Fig. 17.— SEDs for six stars bright at 24 μm found in the the newly identified L1709 aggregate.
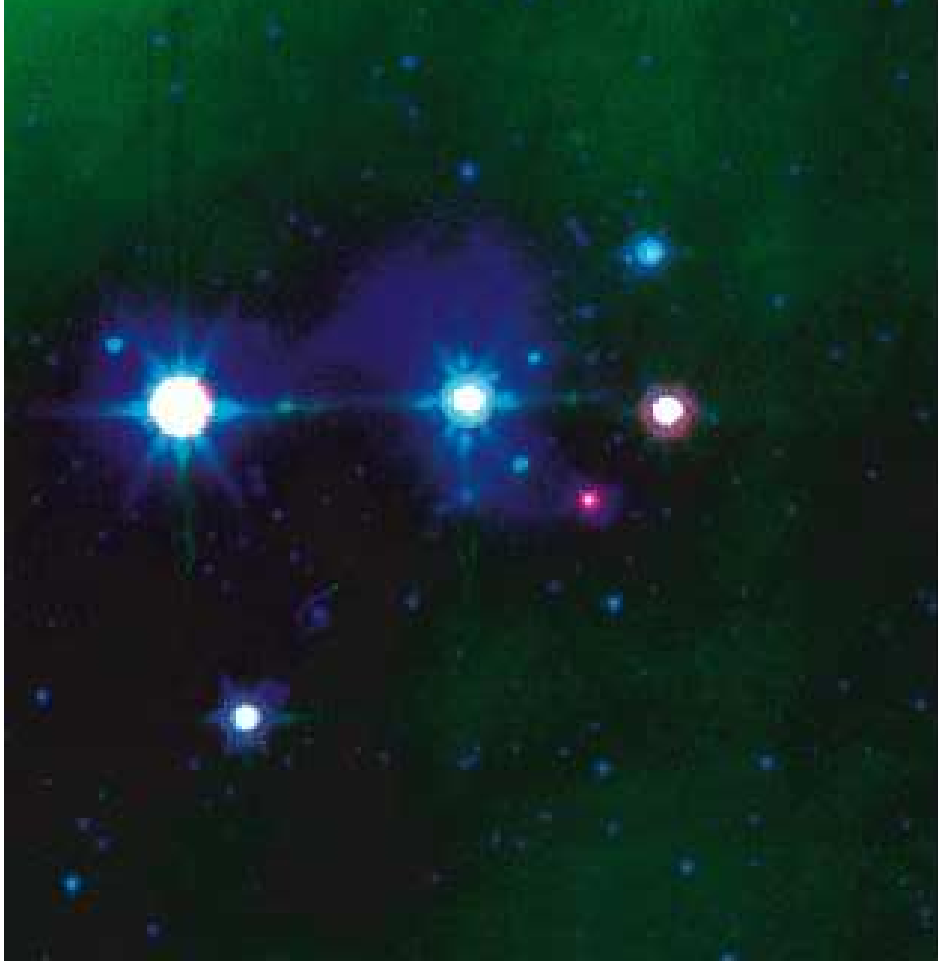
Fig. 18.— Three color 9′ x 9 ′ image of the L1709 aggregate. North is up, and east is left. The IRAC 4.5 μm channel is shown in blue, IRAC 8 μm green, and MIPS 24 μm in red. The candidate edge-on disk (source 5) is clearly extended in the 4.5 μm image.
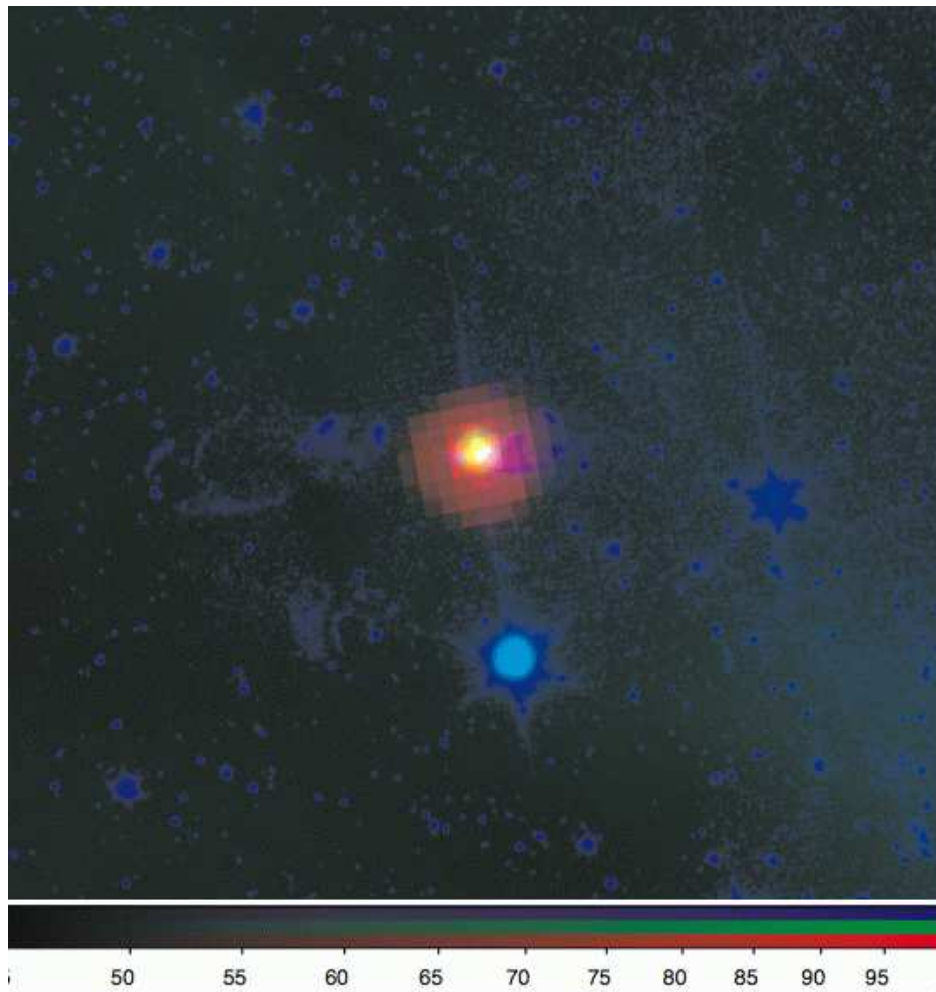
Fig. 19.— Three color 9′ x 9 ′ image of IRAS 16293-2422. The IRAC 8 μm channel is shown in blue, MIPS 24 μm green, and MIPS 70 μm in red. The source is invisible at 8 μm, although the outflow emission and reflection nebulae are visible. Note especially the bow shock features in blue to the left and right of the central source. In this image, north is up, and east is to the left.
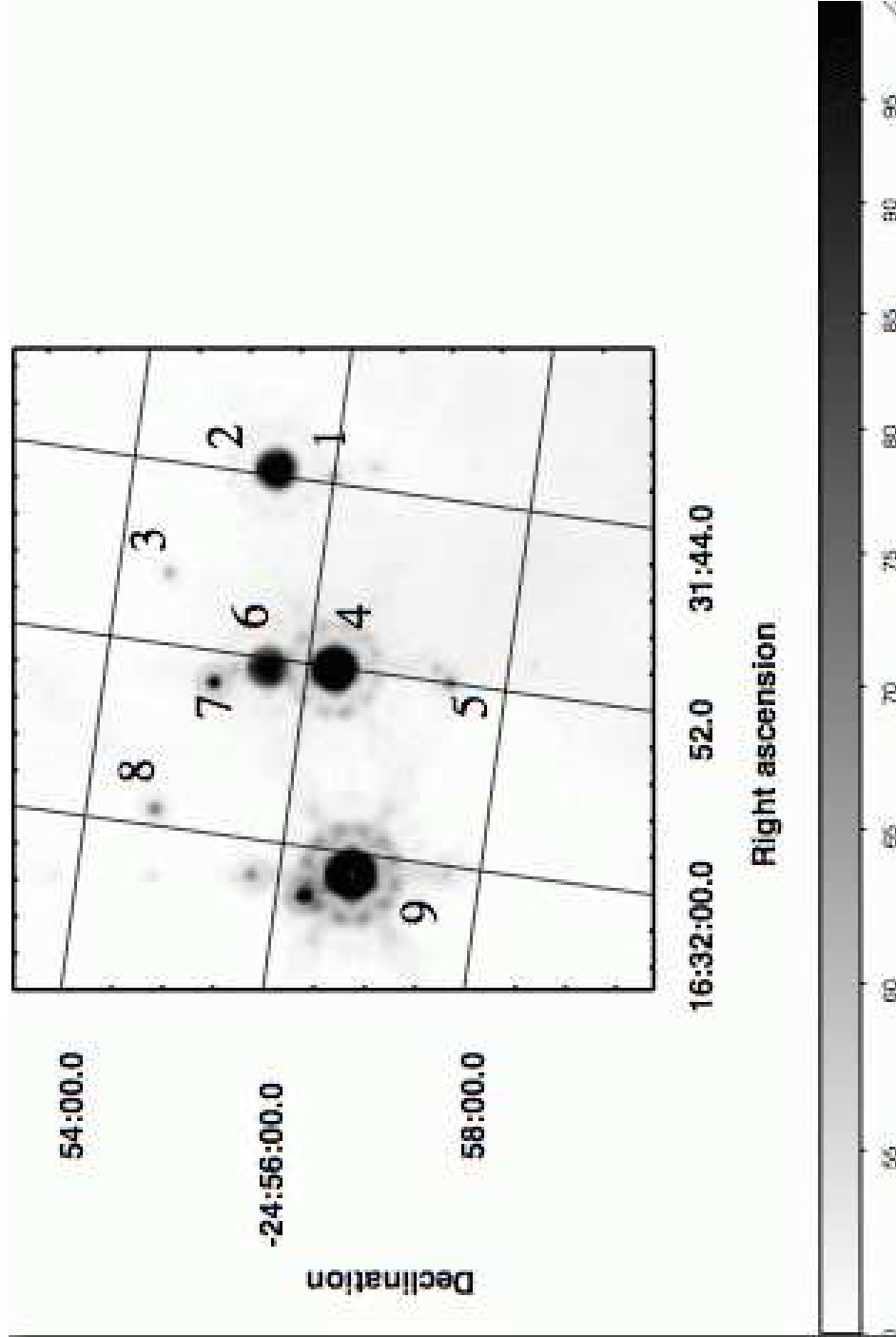
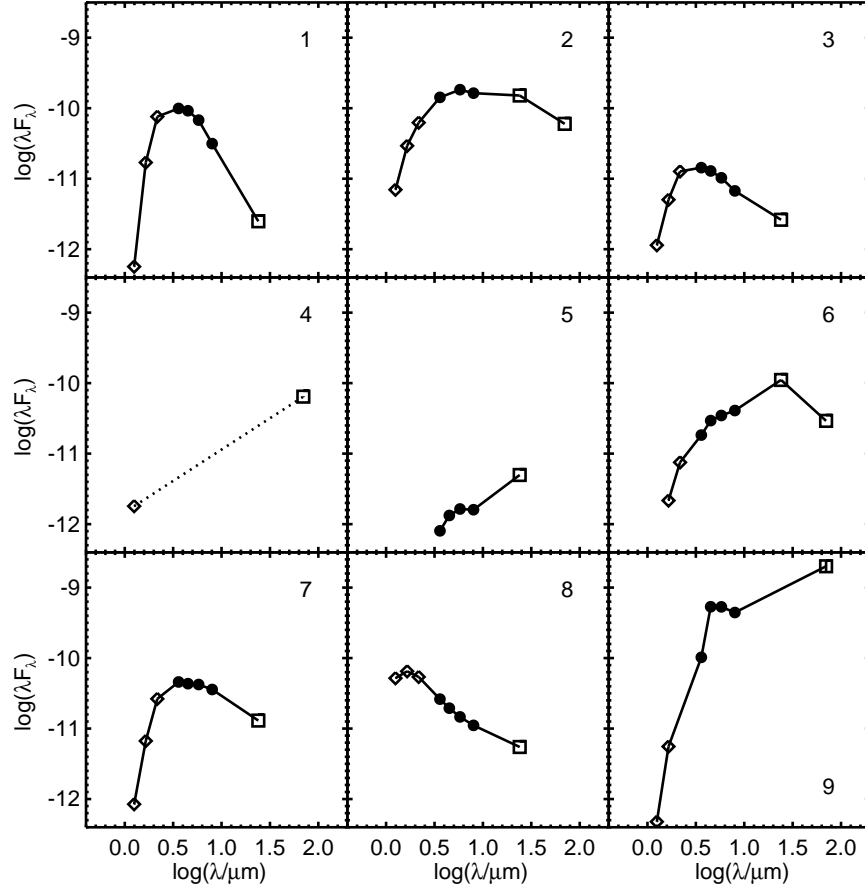Fig. 20.— 24 μm image and finder chart for the L1689 aggregate.

Fig. 21.— SEDs for nine young stellar object candidates bright at 24 μm found tightly clumped together in L1689. Source 4 is saturated in all *Spitzer* bands except 70 μm
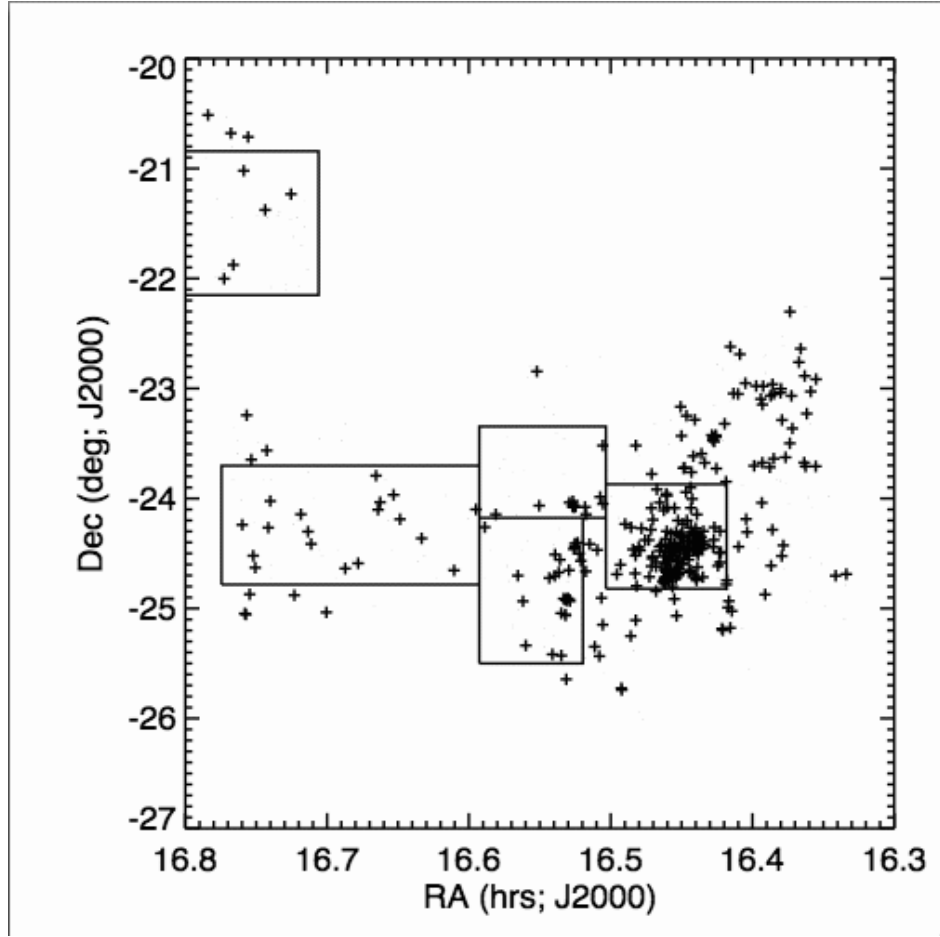
Fig. 22.— Locations of sources where $K_s - [24] > 2$ and $K < 14$.